

# Dynamic fracture of inorganic glasses by hard spherical and conical projectiles

M. Munawar Chaudhri  
Cavendish Laboratory, Department of Physics,  
University of Cambridge,  
J J Thomson Avenue,  
Cambridge CB3 0HE, UK

Electronic mail: [mmc11@cam.ac.uk](mailto:mmc11@cam.ac.uk)

## Abstract

In this article high-speed photographic investigations of the dynamic crack initiation and propagation in several inorganic glasses by the impact of small spherical and conical projectiles are described. These were carried out at speeds of up to  $\sim 2 \times 10^6$  frames  $s^{-1}$ . The glasses were fused silica, 'Pyrex' (a borosilicate glass), soda-lime and  $B_2O_3$ . The projectiles were 0.8 to 2 mm diameter spheres of steel, glass, sapphire and tungsten carbide and their velocities were up to  $340 \text{ m.s}^{-1}$ . In fused silica and Pyrex spherical projectiles' impact produced Hertzian cone cracks travelling at terminal crack velocities, whereas in soda-lime glass fast splinter cracks were generated. No crack bifurcation was observed, which has been explained by the nature of the stress intensity factor of the particle-impact-generated cracks, which leads to a stable crack growth. Crack bifurcation was, however, observed in thermally tempered glass; this bifurcation has been explained by the tensile residual stress and the associated unstable crack growth. A new explanation has been proposed for the decrease of the included angle of the Hertzian cone cracks with increasing impact velocity.  $B_2O_3$  glass showed dynamic compaction and plasticity due to impact with steel spheres. Other observations, such as total contact time, crack lengths, and response to oblique impacts have also been explained.

**Keywords:** *Terminal crack velocity; crack bifurcation; high-speed photography; particle impact; fused silica; Pyrex; soda-lime glass;  $B_2O_3$ ; Hertzian cone crack angle*

## 1. Introduction

Inorganic glasses are highly brittle materials and are prone to being damaged when they are subjected to localised contact loading, quasi-static or dynamic, with hard spherical and pointed projectiles. The nature of the ensuing damage depends on whether the contact is elastic or elastic/plastic.

Quasi-static loading on a glass specimen can be carried out using a mechanical testing machine, whereas impact loading requires a suitable particle propulsion apparatus.

Several investigations of the damage in glass surfaces due to quasi-static loading with hard spheres have been made since the late 19<sup>th</sup> century [1-10]. In these studies the most dominant

aspect of the damage was the Hertzian cone cracking. Early studies of cone cracking in inorganic glasses by impact with hard spheres were made by Raman [11], Benerji [12] and Andrews [13]. Interestingly, all these three authors [i.e. Ref. [11-13]] suggested confidently that the impact-generated cone cracking was due to the shear stresses. However, this view is not now generally held and it is widely accepted that cone cracking is due to the surface radial tensile stress at the circle of contact between the sphere and the target, generated by the impact.

There are, however, relatively few in situ observations from impact loading of glass specimens with spherical or pointed projectiles. The main reason for the paucity of such studies appears to be due to the fact that the total contact time between a test glass surface and the impinging projectile, 1 to 2 mm in diameter, is only about a couple of microseconds. Thus, in order to make in situ observations of a small particle impact on a glass surface and the ensuing damage in the latter, specialised high-speed photographic techniques and particle propulsion methods are required.

Such high-speed photography techniques have been available in the Cavendish Laboratory since the 1950s when the Laboratory obtained a Beckman and Whitley Model 189 rotating mirror high-speed framing camera (Beckman and Whitley Inc., California, USA) capable of recording images at up to  $\sim 2$  million frames per second (private communication, Dr A. D. Yoffe, Cavendish Laboratory (1985)). In the early 1970s a particle propulsion system was designed and constructed [14] in the laboratory, with which it became possible to make investigations of the impact response of a wide range of inorganic glasses [15-20] and ionic crystals [21].

The main aims of this study were (a) to investigate the time sequence of the initiation and growth of the localised damage when small, hard spherical and conical projectiles impact inorganic glass surfaces normally or obliquely at velocities of up to  $300 \text{ m.s}^{-1}$ , (b) to examine the nature of the damage generated, (c) to measure the velocities of the dynamic cracks, and (d) to examine the effects of the residual stress in specimens, especially due to thermal toughening, on the nature of the damage produced.

In this article we describe our experimental work from two ‘anomalous’ and two ‘normal’ glasses. The definitions of ‘normal’ and ‘anomalous’ can be found in Ref.[19]. (Basically, for normal glasses  $1/G.dG/dT$  is negative, whereas this expression is positive for anomalous glasses, where  $G$  and  $T$  are the shear modulus of the glass and the temperature. Moreover, it is well known that when loaded with a Vickers diamond indenter, normal glasses deform by genuine shear, but anomalous glasses deform by the process of compaction.) It is shown below that the particle impact response of anomalous glasses is significantly different from that of normal glasses. Moreover, the experimental results presented below are also particularly relevant to the studies of erosion and strength degradation of solids due to solid particle impact.

## **2. Theoretical background**

### **(a) Elastic regime**

In the case of a solid sphere of radius  $R$  quasi-statically loaded normally to a load  $P$  on to a semi-infinite elastic solid, Hertz [1] was the first to analyse the stresses in the elastic regime. Hertz showed that the contact between the sphere and the elastic half space occurs over a circular disc of radius  $a$  given by Eq. (1)

$$a = \left( \frac{4}{3} \frac{k}{E_1} PR \right)^{1/3}, \quad (1)$$

where

$$k = \frac{9}{16} \left\{ (1 - \nu_1^2) + (1 - \nu_2^2) \frac{E_1}{E_2} \right\}$$

in which  $\nu_1$  and  $\nu_2$  and  $E_1$  and  $E_2$  are the Poisson's ratios and elastic moduli of the half space and sphere, respectively.

Hertz [1] also showed that on the surface of the half space at a distance  $r$  from the point of first contact between the sphere and the half space and outside the contact circle, the radial stress  $\sigma_r$  is tensile and is given by

$$\sigma_r = \frac{1}{2} \frac{P}{\pi r^2} (1 - 2\nu_1). \quad (2)$$

Moreover, on the surface and outside the circle of contact the circumferential stress,  $\sigma_\theta$  is compressive, but it is of an equal magnitude to the radial stress,  $\sigma_r$ .

When the compressive load  $P$  on the sphere is gradually increased, the circle of contact increases according to Eq. (1) and as the applied load reaches a critical value, a ring crack of radius  $r_c$  forms in the surface of the semi- infinite solid. With further increase in the normal load, the ring crack develops into a cone crack (see Fig. 1). The size of the cone crack increases with the applied normal load  $P$  such that  $\frac{P}{S^{3/2}}$  remains constant [4, 6], where  $S$  is the base of the cone crack (see Fig. 1).

Now, when a solid elastic sphere of radius  $R$ , density,  $\rho$ , elastic modulus  $E_2$  and Poisson's ratio  $\nu_2$  strikes normally with an initial velocity  $V$  an elastic half space of Young's modulus  $E_1$  and Poisson's ratio  $\nu_1$ , the quasi-static theory of Hertz [1] is still applicable if the total contact time between the sphere and the half space is longer than the time taken by the dilatational waves to travel through twice the diameter of the impacting sphere.

As shown below, although the successive wave reflections' assumption of Hertz is fulfilled for the impacting sphere, it is clearly not the case for the semi infinite solid. However, from the measurement of the time of collision between a 1.59 mm diameter steel sphere falling freely at a speed of  $3.41 \text{ m.s}^{-1}$  on to a flat end of a steel cylinder 152 mm in diameter and 203 mm in height, it has been shown by Goodier et al.[23] that the Hertz's quasi-static theory correctly predicts the total collision time. On the other hand, the measured maximum impact load was only about 82% of that predicted by the Hertz theory. This discrepancy between the measured maximum impact load and the theoretically predicted load is not necessarily due to the fact that some of the energy is dissipated in the elastic waves, as shown by Hunter [24]. A possible cause is the loss of energy by viscous flow and any plasticity effects.

Ignoring the above discrepancy, according to Hertz [1] the maximum impact-generated load,  $P_{\max}$ , is given by

$$P_{\max} = \left(\frac{5}{3}\pi\rho\right)^{3/5} \left(\frac{4}{3}\frac{k}{E_1}\right)^{-2/5} R^2 V^{6/5} \quad (3)$$

in which all the variables have been defined in the above.

The theoretical maximum elastic impact mean normal pressure,  $p_m$ , is given by

$$p_m = \frac{1}{\pi} \left(\frac{5}{3}\pi\rho\right)^{1/5} \left(\frac{4}{3}\frac{k}{E_1}\right)^{-4/5} V^{2/5} \quad (4)$$

The total theoretical elastic contact time,  $t_{\text{elastic}}$ , between the impacting sphere and the half space is given by

$$t_{\text{elastic}} = 2.94 \left[ \frac{5}{4}\pi\rho \left( \frac{1-\nu_1^2}{E_1} + \frac{1-\nu_2^2}{E_2} \right) \right]^{2/5} \frac{R}{V^{1/5}} \quad (5)$$

### (b) Elastic/plastic regime

If during the sphere's impact with the half space, the latter deforms plastically, then Hertz's equations (1-5) are no longer applicable and a different set of equations as, for example, that developed by Yoffe [25], comes into play. According to Yoffe's model, the new stress field is a combination of the Boussinesq field [26] due to a point loading on the surface of the half space and a localized field due to the plastically deformed zone (or densified/compacted zone in the case of some glasses). Yoffe [25] named this localized field as the 'blister' field, named so as the plastically deformed zone causes 'discomfort' similar to that caused by a blister.

Note that the blister field varies as  $\frac{1}{r^3}$  and thus it is a local one (it may also be noted that the stress field due to the expanding cavity model is also a local one and cannot be applied to the loading of an indenter on a surface of an elastic/plastic solid [25]). The strength of the blister field  $B$  (see Eq. (6) below) is dependent upon the maximum applied load, the capability of the half space to be compacted, and the geometrical shape of the impacting particle. The value of  $B$  can be determined, as shown by Chaudhri [27]. Taking the z-axis along the particle's load axis (also for this direction of z-axis,  $\theta = 0$  and  $\theta = \frac{\pi}{2}$  along the loaded surface), the various principal stresses at a distance  $r$  from the initial point of contact in spherical coordinates during the loading under an applied load  $P$  are

$$\sigma_r = \frac{P}{4\pi r^2} (1 - 7 \cos \theta) + \frac{B}{r^3} (19(\cos \theta)^2 - 7) \quad (6a)$$

$$\sigma_\theta = \frac{P}{4\pi r^2} \left( \frac{(\cos \theta)^2}{1 + \cos \theta} \right) - \frac{B}{r^3} (\cos \theta)^2 \quad (6b)$$

$$\sigma_\phi = \frac{P}{4\pi r^2} \left( \cos \theta - \frac{1}{1 + \cos \theta} \right) + \frac{B}{r^3} (2 - 3(\cos \theta)^2) \quad (6c)$$

On the surface  $z = 0$  and  $\theta = \frac{\pi}{2}$ . Therefore, Eqs. (6 a-c) become

$$\sigma_{r,\frac{\pi}{2}} = \frac{P}{4\pi r^2} - \frac{7B}{r^3} \quad (7a)$$

$$\sigma_{\theta,\frac{\pi}{2}} = 0 \quad (7b)$$

$$\sigma_{\phi,\frac{\pi}{2}} = -\frac{P}{4\pi r^2} + \frac{2B}{r^3} \quad (7c).$$

From Eqs. (7a-c) we note that on the surface the stresses  $\sigma_r$  and  $\sigma_\phi$  can be compressive or tensile, depending upon the values of  $P$  and  $B$ . This suggests that for an elastic/plastic loading of a half space both ring and radial cracks can initiate on the surface.

During the unloading we see from equations (6) and (7) that whereas  $P$  decreases to zero the value of  $B$  remains unchanged. Thus, even before complete unloading (i.e.  $P = 0$ ) a stage is reached when in Eq. (7)  $\sigma_r$  becomes compressive and  $\sigma_\phi$  tensile.

On complete unloading (i.e.  $P = 0$ ), the various principal stresses on the surface (i.e.  $\theta = \frac{\pi}{2}$ ) are

$$\sigma_r = -\frac{7B}{r^3} \quad (8a)$$

$$\sigma_\theta = 0 \quad (8b)$$

$$\sigma_\phi = \frac{2B}{r^3} \quad (8c).$$

We note from Eq. (6) that during loading and for  $\theta = 0$ ,  $\sigma_\theta = \frac{P}{8\pi r^2} - \frac{B}{r^3}$ , which can be tensile and can give rise to a subsurface median crack.

Furthermore, we note from Eq. (6) that on complete unloading and for  $\theta = 0$ ,  $\sigma_r = \frac{12B}{r^3}$ , which is tensile and can give rise to lateral cracking initiating on the load axis.

We have already illustrated schematically ring and cone cracks during the elastic loading of a half space with a hard sphere in Fig. 1. Median, radial and lateral cracks are shown schematically in Fig. 2. It should be noted that in Fig. 2 we have shown an elastic/plastic indentation made with a hard pyramidal indenter of an included angle  $2\psi$ . The picture remains the same when plasticity is caused in the surface by loading with a hard spherical indenter.

The contact time between a spherical projectile and a half space cannot be predicted correctly using Eq. (5) if during the impact, plasticity takes place either in the half space or in the impinging projectile or in both. Therefore, another expression is required in place of that given by Eq. (5). Tabor [28] has given an expression for the plastic loading time  $t_{\text{plastic}}$  in the case of a hard sphere of radius  $R$  and mass  $m$  striking normally a half space of dynamic flow stress  $Y_{\text{dynamic}}$ . Thus,

$$t_{\text{plastic}} = \frac{\pi}{2} \left( \frac{m}{2\pi R Y_{\text{dynamic}}} \right)^{1/2}. \quad (9)$$

Therefore, the total contact time is given by

$$t_{contact} = \frac{\pi}{2} \left( \frac{m}{2\pi R Y_{dynamic}} \right)^{1/2} + 1.47 \left[ \frac{5}{4} \pi \rho \left( \frac{1-v_1^2}{E_1} + \frac{1-v_2^2}{E_2} \right) \right]^{2/5} \frac{R}{V_{rebound}^{1/5}} \quad (10)$$

We note from Eq. (10) that the total contact time,  $t_{contact}$ , is the sum of two components. The first component is independent of the initial impact velocity as long as  $Y_{dynamic}$  remains constant, independent of the strain rate. In the second component the elastic rebound time varies only slowly with the rebound velocity of the projectile.

If on the other hand, the impacting sphere deforms plastically and the impacted glass surface does not, then another expression is needed for the plastic loading time,  $t_{plastic}$ . Andrews [29] has derived an expression for the plastic loading time when two identical soft metal spheres collide along the line of their centres. Thus Andrews [29] gives the expression for the loading time as

$$t_{plastic.sp} = \frac{\pi}{2} \left( \frac{m}{\pi R p_{dynamic}} \right)^{1/2} \quad (11)$$

where  $p_{dynamic}$  is the mean dynamic plastic deformation pressure of the spheres. The expression in Eq. (11) has omitted a numerical factor of 2 in the denominator of the term in the brackets and we can easily derive the correct expression as

$$t_{plastic.sp} = \frac{\pi}{2} \left( \frac{m}{2\pi R p_{dynamic}} \right)^{1/2} \quad (12)$$

Therefore, the total contact time between a plastically deforming metallic sphere and a glass half space is given by

$$t_{plastic.sp} = \frac{\pi}{2} \left( \frac{m}{2\pi R p_{dynamic}} \right)^{1/2} + 1.47 \left[ \frac{5}{4} \pi \rho \left( \frac{1-v_1^2}{E_1} + \frac{1-v_2^2}{E_2} \right) \right]^{2/5} \frac{R}{V_{rebound}^{1/5}} \quad (13)$$

Note that in Eq. (13) we have assumed that during the rebound of the projectile, the glass surface is flat and uncrushed and that the radius of the recovered sphere is the same as that before the impact, even though in reality the unloaded sphere will have a larger radius than originally.

$p_{dynamic}$  in Eqs. (11 – 13) is not constant, but it varies with the dimensionless contact radius  $a/R$ , where  $a$  and  $R$  are the radii of the flat on the sphere and the sphere, respectively, as shown in an experimental study by Chaudhri, Hutchings and Makin [30] in the case of a sphere of phosphor bronze in a heavily work - hardened state which is compressed quasi-statically between two hard platens. These authors reported that when the sphere was gradually compressed by slowly increasing the compressive force, plastic deformation of the sphere first occurred when  $a/R = 0.05$  and the mean deformation pressure was about  $0.6 H_v$  where  $H_v$  is the Vickers diamond hardness of the sphere. The mean plastic deformation reached a peak value of  $\sim 0.8 H_v$  when  $a/R = 0.2$ . With further increase in the compressive force, the mean deformation pressure of the sphere reduced and dropped to values of  $0.66 H_v$

and  $0.42 H_v$  for  $a/R$  values of 0.4 and 0.6, respectively. We assume that in our impact experiments the plastic deformation behaviour of the steel spheres was similar to the response of the phosphor bronze sphere. In our impact experiments with steel spheres (see below), plasticity of the spheres occurred at an impact velocity of greater than  $80 \text{ m.s}^{-1}$  and for impact velocities in the range 200 to  $250 \text{ m.s}^{-1}$  the values of the dimensionless radius  $a/R$  were in the range 0.6 to 0.65, which correspond to dynamic loads of 1170 and 1330 N, respectively.

### 3. Experimental

The projectile impact experiments were carried out on optically polished blocks of pure fused silica (Vitreosil, Thermal Syndicate Ltd. UK), of size 50 mm x 25 mm x 10 mm, Pyrex (a borosilicate glass trademark, Corning Glass, USA) of size 50 mm x 50 mm x 25 mm, soda – lime glass (Pilkington, UK) of size 50 mm x 50 mm x 25 mm, and  $\text{B}_2\text{O}_3$ , which was prepared in the laboratory [19]. Blocks of this glass of size 20 mm x 10 mm x 10 mm were prepared and polished to a good optical finish just before carrying out experiments on them. This was necessary in order to reduce the interaction of the atmosphere with the glass surfaces, which made them translucent and, therefore, difficult to see through clearly. Fused silica and Pyrex glass are anomalous glasses, whereas soda-lime and  $\text{B}_2\text{O}_3$  glasses are normal types [19].

The projectiles were 0.8 and 1.0 mm diameter hardened steel spheres, 1 mm diameter soda-lime glass spheres, 1 mm diameter synthetic ruby spheres, 1 and 2 mm diameter tungsten carbide spheres, and tungsten carbide cones of an included angle of  $90^\circ$  and a base of 1 mm diameter. The apex of the tungsten carbide cones was  $\sim 10 \mu\text{m}$  in diameter, but the surface of the cones was not shiny, as they were made by grinding 1 mm diameter tungsten carbide rods with a fine diamond wheel. The cones were then cut off from the rods, using a fine diamond saw. The surface of the steel, tungsten carbide and ruby spheres was of an optical quality, whereas the surface roughness of the glass spheres was  $\sim 1 \mu\text{m}$ . The surface roughness of the tungsten carbide cones was also about  $1 \mu\text{m}$ . Some relevant physical properties of the various projectiles and glass blocks are given in Table 1.

The projectiles were propelled at velocities of up to  $300 \text{ m.s}^{-1}$ . In most cases the projectiles impacted the targets (i.e. glass blocks) at normal incidence, but in some cases we also investigated oblique impacts. An explosive gun [14] was used for the propulsion of the projectiles. In order to observe in situ the process of impact and ensuing fractures during the various stages of an impact, a high-speed framing camera (Beckman and Whitley model 189, Beckman and Whitley Inc. California, USA) working at framing speeds of up to  $1.7 \times 10^6$  frames per second was used. A schematic diagram of the experimental arrangement used can be found in Ref. [15]. A 35 mm HP5 (Ilford) film was used in the camera. Some photographic sequences were recorded on Kodak VR 1000 colour film (1000 ASA). The event was back-lit with the flash (duration:  $\sim 135 - 140 \mu\text{s}$ ) from a Xenon-filled FA 5 flash tube. In the photographs, this arrangement made the cracks look dark.

Table 1. Some relevant physical properties of the various glasses and projectiles.\*

Physical property	Fused silica (Vitros -il)	Soda – lime glass (Pilkington)	Borosilicate glass (Pyrex)	Borate glass (B <sub>2</sub> O <sub>3</sub> )	Steel spheres	Tungsten carbide spheres	Single crystal sapphire
Young's modulus E / GPa	7.25 x 10 <sup>10</sup>	6.9 x 10 <sup>10</sup>	6.1 x 10 <sup>10</sup>	1.51 x 10 <sup>10</sup>	2.05 x 10 <sup>11</sup>	6.5 x 10 <sup>11</sup>	4.3 x 10 <sup>11</sup>
Poisson's ratio, $\nu$	0.17	0.25	0.22	0.29	0.3	0.26	0.26
Density $\rho$ / kgm <sup>-3</sup>	2.2 x 10 <sup>3</sup>	2.5 x 10 <sup>3</sup>	2.32 x 10 <sup>3</sup>	1.83 x 10 <sup>3</sup>	7.85 x 10 <sup>3</sup>	14.85 x 10 <sup>3</sup>	4.0 x 10 <sup>3</sup>
Longitudinal wave velocity / m.s <sup>-1</sup>	5740	5250	5230	2870	5110	6620	10400
Wave traversal time for a round trip in a 1 mm diameter sphere / $\mu$ s		0.38			0.39	0.3	0.19
Vickers hardness / GPa	7.2	5.4	5.8	1.7	9.2	24.5	23.5 – 29.4

\* All the data in this table are from references [19, 20], except the Vickers hardness value of tungsten carbide, which is from Ref. [31].

After an impact experiment, some of the impacted glass blocks were sectioned through the damage with a fine diamond saw and the sectioned surface was polished and etched (if necessary) in order to examine further the nature of the sub-surface damage.

The error in the measurements of the interframe time of the high-speed photographs was less than 1 %, and the accuracy in the measurements of the crack velocities was  $\pm 100 \text{ m.s}^{-1}$ .

#### 4. Results

We present the results according to the shapes of the projectiles and the type of glasses investigated. Note that here we have presented the high-speed photographic sequences in an orientation in which the projectiles appear to be coming from above, whereas in reality the projectiles were propelled vertically upwards. This is done for an ease of visualization of the

impact and the ensuing damage. Moreover, in the sequences the various crack systems have been identified with reference to Figs. 1 and 2.

### **(a) The impact of spherical projectiles on anomalous glasses**

A general observation from the impact experiments on anomalous glasses was that for all impact velocities used, Hertzian cone cracks formed in both fused silica and Pyrex glasses. However, in both these glasses the included angles of the cone cracks formed were significantly smaller than the included angles of the cones formed under quasi – static loading.

A sequence of high-speed photographs of the impact of a 1 mm diameter steel sphere at normal incidence on a block of Pyrex glass at  $160 \text{ m.s}^{-1}$  is shown in Fig. 3. The impact occurs between frames 2 and 3 and the ensuing cracks in the Pyrex glass block formed about 0.1 to 0.2  $\mu\text{s}$  before frame 3. The uncertainty in the moment of contact is due to the fact that at a framing rate of  $1 \mu\text{s}$  per frame the exposure time of each frame is  $1/6^{\text{th}}$  of the inter-frame time. It will be seen in frame 3 that a cone crack of a semi-included angle of  $43.5^\circ$  has already formed just below the contact between the projectile and the glass and its length, as measured along the skirt of the cone, is approximately 0.35 mm. Therefore, the velocity of this cone crack is 3500 to 1800  $\text{m.s}^{-1}$ . In frame 4 the cone crack has already reached the bottom of the frame, which means that between frames 3 and 4 the cone crack velocity is at least 2500  $\text{m.s}^{-1}$ . Note that the included angle of the cone crack remains the same as the angle in frame 3. It will also be seen from frame 4 that on the left of the impact site a radial crack, R, has formed. Another point to note is that in this frame the cone crack appears dark, which means that the flanks of the cone crack are slightly lifted upwards relative to the impacted surface, which reduces the transmission of the light from the flash tube. However, in the very next frame the flanks of the cone crack start closing up with the result that more light is transmitted through the crack system. We estimate that the sphere leaves the surface of the Pyrex block about 0.1  $\mu\text{s}$  before frame 5, thus giving a total contact time of about 2  $\mu\text{s}$ . Note also that during the rebound of the sphere a lateral crack has opened up on the left of the impact site, but the radial crack, R, has closed up, not healed. Moreover, the flanks of the cone crack have risen up again, resulting in reduced transmission of light. The opening and closing of the flanks of the cone crack continues at a frequency of  $5 \times 10^5 \text{ s}^{-1}$  up to at least frame 10.

We also note from frames 8 to 10 that following behind the rebounding sphere, some broken up glass is thrown normally upwards from the impact site at  $\sim 70 \text{ m.s}^{-1}$ . The rebound velocity of the sphere is  $120 \text{ m.s}^{-1}$ .

A photographic sequence, taken at a framing rate of  $1.7 \times 10^6$  frames per second, of the formation and growth of damage in another anomalous glass, namely fused silica, when it was impacted normally with a 1 mm diameter tungsten carbide sphere at a velocity of 200  $\text{m.s}^{-1}$  can be found in Ref. [18]. In this case both cone and median cracks travelling at a maximum velocity of  $(2350 \pm 40) \text{ m.s}^{-1}$  formed and developed. This crack velocity is about

10 % higher than the maximum crack velocity reported by Schardin [32] from his tensile experiments. In our experiments we did not observe any crack bifurcation.

### **(b) Normal glasses**

In this section we shall give two examples from normal glasses. Fig. 4 shows a sequence of photographs when a polished block of soda-lime glass is impacted at normal incidence with a 0.8 mm diameter steel sphere at a velocity of  $300 \text{ m.s}^{-1}$ . The impact occurs  $0.6 \mu\text{s}$  after frame 1. This immediately leads to the creation of jets of fine debris of glass particles travelling in the air at speeds of up to  $600 - 700 \text{ m.s}^{-1}$ . Within the glass block itself fast finger-like cracks travelling at  $\sim 1500 \text{ m.s}^{-1}$  are generated. From this sequence of photographs it is not clear whether any cone cracks are formed before the generation of the finger – like cracks. However, other photographic sequences have shown that when a 2 mm diameter tungsten carbide sphere impacted a block of soda – lime glass at normal incidence at a velocity of  $130 \text{ m.s}^{-1}$ , first a cone crack is formed which is rapidly followed by fast finger – like cracks (or splinter cracks) (sequence not shown here).

In frame 3 of Fig. 4 a median crack, M, is shown along the load axis. Although in this frame the glass debris obscures the impacting sphere, it appears that the sphere has begun its rebound with the formation of lateral cracks (see at L in frame 3). The lateral cracks continue to grow in frames 4 and 5. When some of these lateral cracks reach the impacted surface, chips of the detached glass are formed. One such a chip is shown in frame 12, which is about  $11 \mu\text{s}$  after the initial impact.

The second example showing the response of another normal glass to impact with a spherical projectile is presented in Fig. 5. Here a 1 mm diameter steel sphere impacts at normal incidence a block of the  $\text{B}_2\text{O}_3$  glass at a velocity of  $150 \text{ m.s}^{-1}$ . The contact between the sphere and the  $\text{B}_2\text{O}_3$  block occurs in frame 3. No cracks appear to form during the loading period, but some densification takes place, which can be seen at the arrow in frame 3. In fact, within this densified zone two white arcs appear. A possible cause for the appearance of the arcs may be the refraction of the transmitted light through the densified zone. Unloading begins between frames 4 and 5 and several radial and lateral cracks form (see frame 5), which continue to grow for another  $\mu\text{s}$  after the sphere has left the surface of the glass block (see at L in frame 6). It will also be seen that in frame 5 a dark protrusion has just appeared on the glass surface around the contact during the unloading (i.e. rebound) of the sphere. This dark protrusion is, in fact, a ring of detached  $\text{B}_2\text{O}_3$ , which leaves the impact surface in a direction normal to it at a velocity of  $135 \text{ m.s}^{-1}$  and a dent is left behind in the glass surface. This rebound velocity of the sphere is relatively high, being about 85% of the incident velocity. This relatively high rebound velocity is reasonable, as little or no loss of energy occurs because of the absence of any cracking during the loading part of the impact.

It is interesting to mention that if  $\text{B}_2\text{O}_3$  is mixed with 32.5 % by weight of  $\text{Na}_2\text{O}$ , the response of the resulting glass is quite similar to that of soda-lime glass [19].

### **(c) Variation of the Hertzian cone angle with the projectile impact velocity**

Previously [16], we reported that the included angle of the Hertzian cone crack in Pyrex glass decreased with increasing impact velocity with the 1.0 and 0.8 mm diameter hardened steel projectiles. For example, the semi - included angles of the Hertzian cones in Pyrex for impact velocities of  $\sim 95$  and  $240 \text{ m.s}^{-1}$  were  $55^\circ$  and  $35^\circ$ , respectively. The semi included angle of the Hertzian cone crack in Pyrex produced by quasi-static loading with a hard sphere is  $62.5^\circ$ . Our experiments have shown that both soda – lime glass and fused silica glass also show a similar response. However, we are not certain if impacts at velocities greater than  $180 \text{ m.s}^{-1}$  produce any Hertzian cone cracks in soda – lime glass. On the other hand, in fused silica, cone cracks formed up to the highest impact velocity of  $320 - 340 \text{ m.s}^{-1}$  studied. Fig. 6 (a – c) shows some typical Hertzian cones in blocks of fused silica produced by impacts with 1 mm diameter steel spheres at velocities of (a) 25, (b) 155, and (c)  $310 \text{ m.s}^{-1}$ . The semi-included angles at these velocities were measured to be  $68.5^\circ$ ,  $46^\circ$ , and  $32.5^\circ$ , respectively. It would be interesting to see if Hertzian cone cracks still form in fused silica and Pyrex when 1 mm diameter steel spheres impacted blocks of these glasses at  $500 \text{ m.s}^{-1}$ .

Hertzian cone angle variation with impact velocity was also observed for the fused silica with 1 mm diameter projectiles of soda – lime glass and sapphire. Collective data are shown in Fig. 7. In this figure the solid line is drawn through the steel sphere data points. The points corresponding to the glass projectiles lie above the line, whereas those due to the sapphire projectiles agree with those for the steel projectiles up to impact velocities of  $170 \text{ m.s}^{-1}$ , above which the Hertzian cones are narrower with the sapphire projectiles. Fig. 7 also shows the experimental quasi – static value of  $(62.8^\circ \pm 1.2^\circ)$  for the Hertzian cones produced by a 1 mm diameter steel spheres (It may be remarked that the theoretical semi – included angle of the Hertzian cone crack in fused silica for  $v = 0.17$  is  $\sim 53^\circ$ , which is considerably smaller than the experimental value. Interestingly, this problem also exists in the case of the Hertzian cone cracks in soda – lime glass. So far, no satisfactory explanation of this discrepancy has been put forward.).

### **(d) Oblique impact of tungsten carbide spheres on blocks of soda-lime glass**

Quite frequently, the impact angle between a target surface and a projectile is not along the surface normal to the impacted block. In such a situation what is the nature of the damage produced by a projectile impact? To investigate this question, 2 mm diameter tungsten carbide projectiles were propelled on to blocks of polished soda lime glass at several angles to the surface normal at impact velocities in the range of  $125 - 150 \text{ m.s}^{-1}$  and the ensuing damage was photographed at  $10^6 \text{ frames s}^{-1}$ . It was found that the main characteristics of the damage were quite similar to those produced by normal impacts. However, there was one significant difference; for oblique impacts the resulting Hertzian cone cracks were not oriented symmetrically to the target's surface normal. In fact, it was found that as the angle of impact decreased from  $90^\circ$  (i.e. being along the surface normal), that between the axis of the resulting Hertzian cone fracture and the normal to the impact surface increased in the projectile's forward direction.

An example of an oblique impact is shown in Fig. 8. A 2 mm diameter tungsten carbide sphere impacts a polished block of soda – lime glass with the angle between the surface normal and the projectile impact direction being  $\sim 60^\circ$ . In this experiment the test glass block was placed between circular polarisers so as to be able to see the behaviour of the isochromatics during the impact. The component of the impact velocity along the surface normal is  $63 - 75 \text{ m.s}^{-1}$  and that along the surface of the glass block is  $108 - 130 \text{ m.s}^{-1}$ . The latter causes the sphere to slide along the glass surface.

The impact of the sphere on the block occurs between frames 2 and 3 and as a result a cone crack appears in frame 3, along with the formation of the isochromatics below the contact region. Note that in this frame the isochromatics are oriented symmetrically to the surface normal through the point of first contact between the sphere and the glass block. The velocity of the cone crack, as measured along the skirt of the front of the cone crack in frame 3, is at least  $600 \text{ m.s}^{-1}$ . In frame 4 the cone crack has become well developed and the front and rear parts of the skirt of the cone crack make angles of  $40^\circ$  and  $22^\circ$ , respectively with the glass surface. Moreover, the speed of the front part of the skirt of the cone crack is  $\sim 950 \text{ m.s}^{-1}$ . A median crack has also appeared inside the cone crack in this frame. Note that although between frames 3 and 4 the isochromatics have enlarged, they still remain symmetrically oriented to the surface normal. This suggests that possibly the dynamic coefficient of friction between the tungsten carbide sphere and the soda-lime glass surface is quite low and does not lead to a significant shear stress on the glass surface. From frames 5 to 9 the inclination of the front part of the cone gradually increases to  $45^\circ$ , whereas the rear part of the cone grows in such a way as to reduce its inclination to the glass surface to about  $18^\circ$ .

Beyond frame 9 there does not appear to be any change in the inclination of the Hertzian cone crack to the glass surface, but a jet of fine glass debris can be clearly seen being ejected from the contact region. The speed of the jet of debris in the forward direction is  $300 \text{ m.s}^{-1}$ . Moreover, it will be seen from frames 3 – 12 that the tungsten carbide sphere slides on the glass surface at a speed of  $50 - 60 \text{ m.s}^{-1}$  and that during this time the sphere does not leave the glass surface.

Thus the situation is that the sphere is loaded dynamically on to the glass block in the presence of a tangential force generated by the sliding of the sphere on the surface. If at any instant of time the dynamic load normal to the glass surface is  $P_1$  and the tangential force due to the sliding of the sphere is  $\mu P_1$ , where  $\mu$  is the coefficient of friction between the tungsten carbide sphere and the smooth surface of soda-lime glass block, the resultant force  $P_2$  is given by

$$P_2 = P_1 (1 + \mu^2)^{1/2} \quad (14)$$

Jelagin and Larsson [10] have measured the coefficient of friction between a tungsten carbide sphere and a smooth surface of soda – lime glass and give a value of  $\mu = 0.13$ . This means that the resultant force  $P_2$  will be inclined to the surface normal at an angle  $\beta$ , where  $\tan\beta = 0.13$ , or  $\beta = 7.4^\circ$ . As stated in the above, the coefficient of friction in our impact experiment is

lower still because the isochromatics remain symmetrically oriented to the surface normal (see frames 3 and 4).

It may be noted that in the case of a Hertzian cone crack formed due to the sliding of a sphere on a surface under a normal load, it has been suggested [33] that because of the tilt of  $P_2$  to the surface normal the axis of any Hertzian cone crack formed will be along  $P_2$ , which means that the front part (in the direction of sliding) of the skirt of the cone crack will make a smaller angle to the glass surface than the rear part of the skirt of the cone crack. The high-speed photographic sequence presented in Fig. 8 shows the inclination of the Hertzian cone crack being opposite to the suggestion made in Ref. [33]. As suggested by us earlier [34], the orientation of the cone crack is controlled by the fact that after the formation of the ring crack under the impacting sphere, the contact disc between the sphere and the glass surface covers more and more of the front part of the ring crack due to the sliding and at the same time the rear part of the ring crack will be covered less and less by the contact disc. This means that the front part of the Hertzian cone crack will grow along steeper stress trajectories than the rear part of the cone. As a result the front part of the cone crack will make a larger angle with the impact surface than will the rear part of the cone.

#### **(e) Conical and sharp-edged projectiles**

Fig. 9 shows a photographic sequence of the impact at normal incidence of a tungsten carbide cone on a polished block of fused silica at a velocity of  $170 \text{ m.s}^{-1}$ . The diameter of the base of the cone is 1 mm and the diameter of the apex of the cone is  $\sim 10 \text{ }\mu\text{m}$ . The apex of the cone makes contact with the fused silica block between frames 1 and 2 and in frame 2 a median crack has appeared just below the contact and its velocity is at least  $2500 \text{ m.s}^{-1}$ . In frame 2 the apex of the cone has penetrated the fused silica block by about  $130 \text{ }\mu\text{m}$ . In the next frame the tungsten carbide cone penetrates further into the fused silica block and the median crack has grown further at  $\sim 1400 \text{ m.s}^{-1}$ . Moreover, the geometrical shape of the median crack changes towards part of a disc and becomes semi circular in frame 4 (see at M in frame 4). Between frames 3 and 4 although the rebound of the projectile has started, the median crack M continues to grow further along the impact axis at  $\sim 950 \text{ m.s}^{-1}$ . In frame 4 a lateral crack has appeared on the left of the impact site. Unloading continues in frames 5 and 6 along with further growth of the lateral crack shown in frame 4 and the generation of more lateral cracks. Moreover, fine glass debris can be seen being ejected along the surface of the tungsten carbide cone at  $\sim 400 \text{ m.s}^{-1}$ .

Views of the top and sectioned surface of the fused silica specimen showed that the median crack was reasonably planar and that there was no indication of crack bifurcation. Moreover, there was no cone crack formation in the fused silica under the tip of the impacting cone. This is an important observation, as it contradicts the observation reported by Hagan [35], who observed a cone crack in a fused silica block when it was quasi-statically loaded with a Vickers diamond indenter.

From the photographic sequence shown in Fig. 9 we have made an estimate of the fracture surface energy of fused silica by using a quasi – static approximation to the dynamic

situation. A value of  $\leq 1.1 \text{ J.m}^{-2}$  is obtained, which is considerably smaller than the value of  $14.1 \text{ J.m}^{-2}$  obtained from quasi-static conical indentations [18] and the value of  $4.42 \text{ J.m}^{-2}$  reported by Wiederhorn [36] from double cantilever experiments at room temperature.

The response of a block of soda – lime glass to a normal impact with a sharp – edged projectile is shown Fig. 10. Here the impact velocity is  $140 \text{ m.s}^{-1}$  and the projectile is a tungsten carbide cone of an included angle of  $90^\circ$ . During its 11 mm flight this projectile oriented itself so that at the moment of impact it was moving with its base (diameter 1 mm) normal to the glass block. The impact occurs in frame 3. We cannot say with certainty whether any cracks have been initiated in this frame. However, in the very next frame three planar cracks, 1 – 3, are formed, with crack number 2 being in the same plane as the base of the cone. Before the impact there was very little rotation of the cone. In frame 3 the base of the cone becomes inclined towards the left of the surface normal to the impact surface by about  $5^\circ$ . Up to frame 6 the projectile maintains this orientation, but then from frame 7 onwards the cone rotates anticlockwise and in frame 12 the base of the cone tilts at an angle of  $62^\circ$  to the specimen surface normal.

In frame 3 the velocity of crack 2 is  $1000 - 1200 \text{ m.s}^{-1}$ , whereas the velocities of cracks 1 and 3 are  $950$  and  $940 \text{ m.s}^{-1}$ , respectively. Between frames 4 and 5 further growth of cracks 1, 2 and 3 occurs at velocities of  $950$ ,  $350$  and  $150 \text{ m.s}^{-1}$ , respectively. Moreover, in frame 5 a fourth crack, lying between cracks 1 and 2 has appeared. The velocity of this fourth crack is at least  $700 \text{ m.s}^{-1}$ . As regards the origins of these four cracks, number 2 is coplanar with the base of the tungsten carbide cone and is a median type (see Fig. 2). We are, however, not clear about the origins of cracks 1 and 3 apart from noting that both these cracks initiate at the surface of the glass block and both these cracks are symmetrically inclined to the impact surface at  $\sim 42^\circ$ . Another notable point is that both cracks 1 and 3 seem to have been initiated at distances of  $0.17$  and  $0.083 \text{ mm}$ , respectively from the initial point of contact between the wedge and the glass surface.

Between frames 5 and 6 cracks 1 and 2 grow at velocities of  $300$  and  $200 - 250 \text{ m.s}^{-1}$ , but there is very little growth of cracks 3 and 4. An interesting point to note in frame 5 is that on the right of the tungsten carbide cone a dark protrusion has appeared, which continues to grow at about  $200 \text{ m.s}^{-1}$  right through to frame 12 in which the protrusion has taken the shape of a possible machined chip. It will also be seen from frames 6 to 12 that the tungsten carbide cone, while dug into the glass block, starts rotating in an anticlockwise direction and by frame 12 the projectile cone has rotated by  $62^\circ$ . It seems possible that that it is the rotation of the tungsten carbide cone, which is the cause of the machined chip. This photographic sequence shows the complexities of the nature of the damage produced, including possible machining, when brittle materials are subjected to sharp – edged projectiles. Moreover, such a complex damage produced by dynamic loading cannot be accounted for using quasi-static theories. It may also be stated that we are not certain whether any melting of the glass occurs around the impact site. We believe, however, that any temperature rise generated by plastic flow will be less than that caused by friction between the projectile and the glass.

#### **(f) Total contact time and crack lengths**

For every normal impact with a spherical projectile on to a glass surface the total contact time between the projectile and the target was obtained from the corresponding high – speed photographic sequence. Every sequence was printed at a suitable magnification and measurements of the position of the projectile with respect to the target surface were made from the prints. From such measurements the total contact time between the projectile and the target surface and the final crack lengths of the damage produced were determined. Thus, some selected data showing the total contact times measured for different targets/spherical projectiles are shown in Table 2. Also shown in Table 2 are the incident and rebound velocities of the projectiles and the total contact times as calculated using Eq. (13).

Table 2. Comparison of measured and calculated total contact times for 1 mm diameter steel spheres of different velocities impacting at normal incidence blocks of fused silica, soda – lime glass and Pyrex (a borosilicate glass).

Projectile material	Target glass	Incident velocity / m.s <sup>-1</sup>	Rebound velocity / m.s <sup>-1</sup>	Total contact time / $\mu$ s	
				Observed	Calculated
steel	Fused silica	135	120	1.9 $\pm$ 0.2	2.2
steel	Fused silica	210	105	2.1 $\pm$ 0.2	2.2
steel	Fused silica	180	140	1.7 $\pm$ 0.2	2.1
steel	Soda – lime glass	180	135	1.5 $\pm$ 0.3 <sup>(a)</sup>	2.2
steel	‘Pyrex’ (borosilicate glass)	160	120	2.0 $\pm$ 0.3 <sup>(a)</sup>	2.2

<sup>(a)</sup> – From Ref. [17]

Crack lengths generated in various blocks of glasses were also measured immediately after the experiment using an optical microscope. When the impact-generated damage was in the form of a Hertzian cone crack, the crack length was measured along the skirt of the cone. On the other hand, when the damage was in the form of splinter–type or finger–type cracks, the measured crack length was that of the longest splinter–type or finger–type crack. The crack lengths data thus obtained are shown in Table 3. In Table 3,  $K_{IC}$  is the critical stress intensity factor.

It will be seen from Table 3 that we have given estimated values of the maximum impact generated loads in column 6. This estimate was made on the basis of the measured flats on the deformed steel spheres due to the impact and knowledge of the variation of the mean deformation pressure of the steel spheres for different  $a/R$  values, as determined from quasi-static compression experiments.

It is interesting to note that the maximum crack lengths in fused silica are about 1.6 times larger than the maximum crack lengths generated in soda – lime glass under similar impact conditions. This ratio is similar to the ratio of the maximum crack velocities in these two glasses.

Table 3. Maximum measured crack lengths in fused silica and soda-lime glass produced by impact with 1 mm diameter steel spheres at velocities of 310 and 330 m.s<sup>-1</sup>, respectively.

Target material	Impact velocity / m.s <sup>-1</sup>	Type of damage	Maximum crack length / mm	Maximum observed crack velocity / m.s <sup>-1</sup>	Maximum estimated impact load / N	K <sub>1C</sub> / 10 <sup>5</sup> Nm <sup>-3/2</sup>
Fused silica	310	Hertzian cone crack	3.44	2500*	1170 - 1330	7.98 <sup>(a)</sup>
Soda – lime glass	330	Splinter – type crack	2.17	1500 – 1550*	1170 - 1330	7.58 <sup>(a)</sup>

\*- This work

<sup>(a)</sup> – From Ref. [36]

### (g) Spherical projectile impact on thermally tempered soda – lime glass

In the photographic sequences presented so far, the target glass samples were stress – free and fast cracks generated in them due to spherical particle impact, were Hertzian cones (in anomalous glasses) and splinter cracks (in soda – lime glass). We did not observe any crack bifurcation either of the cone cracks or of the splinter cracks even though they travelled at, or close to, the terminal velocities. In these sequences the stress intensity factor was such as to lead to a stable crack growth. This means that the length of a crack generated is controlled by the maximum impact load. The question was whether we would observe any crack bifurcation if the stress intensity factor driving the cracks increased with increasing crack length for a constant tensile stress field.

To investigate this possibility, we conducted spherical particle impacts on blocks of thermally tempered soda – lime glass of dimensions 50 mm x 40 mm x 10 mm having a surface compressive stress of 200 MPa. Under this compressive stress the magnitude of the maximum tensile stress inside the blocks is 100 MPa. First we fired 1 mm diameter tungsten carbide spheres at normal incidence on a 50 mm x 10 mm face of a tempered block at velocities of up to 250 m.s<sup>-1</sup>, but the damage was not significant. However, when we fired a 2 mm diameter sphere at a 50 mm x 10 mm face of a block of the tempered glass at a velocity of 150 m.s<sup>-1</sup>, the damage was catastrophic. A typical sequence of photographs is shown in Fig. 11.

In this sequence (i.e. Fig. 11) the test block is placed between two circular polarisers, which cause colour fringes to appear. Each colour fringe represents a constant difference between the principal stresses in a plane normal to the optical axis of the camera. The black fringe in frame 1 represents a region in the glass block where the compressive stress changes to tensile stress. A 2 mm diameter tungsten carbide sphere impacts the tempered glass block at 150 m.s<sup>-1</sup> and the contact between the sphere and the glass surface occurs in frame 3, which results in the generation of splinter cracks (see frame 4). Between frames 4 and 5 the velocity of the splinter cracks is 1500 m.s<sup>-1</sup>. Moreover, the splinter cracks enter the tension zone

between frames 4 and 5. This leads to the initiation of the catastrophic failure of the glass, with the process of fracture being propagated and controlled by the tensile stress present in the glass. In fact, from frame 5 to frame 12 the fracture spreads almost throughout the glass block, showing repeated crack bifurcation. Note that this crack propagation behaviour is quite different from the particle-impact-generated fracture behaviour in stress – free blocks of soda – lime glass.

## 5. Discussion

In this work several aspects of dynamic crack initiation and propagation in inorganic glasses due to small particle impact have been examined experimentally using high-speed framing photography. We shall discuss below each of these aspects separately.

First, we consider the results from the 1 mm diameter steel spheres' impact on various glasses. It was found that in all glasses examined, except the  $B_2O_3$ , Hertzian cone cracks formed for impact velocities of up to  $\sim 180 \text{ m.s}^{-1}$ . Above this velocity, for example for a velocity of  $200 \text{ m.s}^{-1}$ , the response of the anomalous glasses, Pyrex and fused silica, was quite different from the response of the soda – lime glass (a normal glass). Whereas in Pyrex Hertzian cone cracks formed (Figs. 3 ), there were no cone cracks formed in the soda – lime glass and instead splinter – type cracks formed (Fig. 4). In fact, in fused silica Hertzian cone cracks formed even at the maximum projectile velocity of  $\sim 330 \text{ m.s}^{-1}$ . In the case of the Pyrex, Hertzian cone cracks formed at the maximum impact velocity of  $250 \text{ m.s}^{-1}$  used [16]. Another anomalous glass, namely  $Ge_2O$ , has also shown a similar response [19]. The formation of the Hertzian cone cracks due to impacts at relatively high velocities would suggest that the anomalous glasses behaved as if they were elastic. In the case of the impacts with the steel spheres, the maximum impact pressure is expected to rise to  $\sim 0.8 \times H_v$  [30], where  $H_v$  is the Vickers hardness of the steel spheres, if we liken the plastic deformation behaviour of an impacting sphere to that of a sphere being compressed quasi-statically between two hard platens. Now,  $H_v$  of the steel spheres is 9.2 GPa (Table 1). Therefore, the maximum deformation pressure generated on impact with a steel sphere on to a block of Pyrex or fused silica would be  $0.8 \times 9.2 = 7.36 \text{ GPa}$ . In the case of the steel spheres, it is unlikely that the high strain rates prevailing during an impact will cause any significant increase in the yield stress (or the hardness) of the steel, as has been shown by Davies [38]. On the other hand, in the case of soda – lime glass, Gunasekera and Holloway [39] have shown that the indentation hardness of this glass increased by a factor of 3 when the loading time reduced from 60 s to  $10^{-3} \text{ s}$ . Since in our impact experiments the loading times are only about 1 – 2  $\mu\text{s}$ , further increase in the dynamic indentation hardness of the soda – lime glass may be expected.

Although at present there is little or no information available in the open literature on the dynamic hardness of fused silica and Pyrex, it seems quite likely that the indentation hardness of these anomalous glasses will also increase. Therefore in the case of an impact with a 1 mm diameter steel sphere on fused silica, Pyrex, or soda – lime glass, plasticity is not expected. It may be added here that in the case of the impact of a 1 mm diameter tungsten carbide sphere on a block of fused silica at a velocity of  $200 \text{ m.s}^{-1}$ , a maximum pressure of 14.6 GPa would

occur, as calculated using Eq. (4). But crushing of the silica in the contact zone is unlikely to allow the pressure to reach this value.

Furthermore, it is observed that crushing of all three glasses below the contact between the impacting sphere and the test block does take place, but the degree of the crushing varies with the type of glass. Crushing is much more extensive in soda – lime silica glass than in fused silica or Pyrex. It may be said that the stiffness of the glasses in the crushed state will be less than that of the glasses in their intact state. It seems possible that in the crushed state any further dynamic loading is likely to cause the material to deform in a somewhat similar manner to the deformation behaviour of a plastically deforming solid, supporting shear deformation. As a consequence, in impact loading the material below the impact will flow rapidly forming jets of material, as we see in the case of an impact of a 1 mm diameter steel sphere on soda – lime glass (Fig. 4).

An important difference between soda – lime glass and the two anomalous glasses Pyrex and fused silica is that the latter possess an ‘open’ structure. (The density of fused silica is  $2.2 \times 10^3 \text{ kg. m}^{-3}$ , whereas the density of crystalline quartz is  $2.67 \times 10^3 \text{ kg.m}^{-3}$ . This relative low density of fused silica gives rise to an ‘open’ structure, with all the bonds intact. Pyrex glass also has a low density of  $2.23 \times 10^3 \text{ kg.m}^{-3}$ . On the other hand, soda-lime glass is a modified form of silica containing several oxides as fillers. These oxides are  $\text{Na}_2\text{O}$ ,  $\text{CaO}$ ,  $\text{MgO}$  and others. The density of soda-lime glass is  $2.48 \times 10^3 \text{ kg.m}^{-3}$  and it is a ‘filled’ structure’.). This means that any localised stress, such as that produced by an impact with a steel sphere, can be accommodated with the rotation of strong covalent bonds [19] in fused silica. This will lead to some densification and compaction. On the other hand, soda – lime silica is a ‘filled’ structure and when a localised compressive stress is applied, the glass will tend to deform by the process of genuine shear [40] rather than by compaction. The tendency in soda – lime glass to shear under applied local stress would also encourage jetting.

The behaviour of the  $\text{B}_2\text{O}_3$  glass to impact with a steel sphere is quite unusual. It is a normal glass, but it is relatively soft having a Vickers hardness of 1.7 GPa (Table. 1). When impacted with a 1 mm diameter steel sphere at a velocity of  $150 \text{ m.s}^{-1}$ , no cracks of any type formed during the loading part of the impact. Moreover, under the impacting sphere it appeared to densify considerably. However, during the rebound of the projectile, the densification partially recovered and then as soon as the projectile left the surface of the glass, radial and lateral cracks formed, as would be expected from the elastic/plastic model given in section 2 (b). The ring of material that detaches during the rebound of the impacting sphere had, in fact, piled up around the sphere, as if it flowed plastically [41], during the loading part of the impact (see Fig. 5, frame 3) and then detached from the glass surface as the steel sphere started its rebound.

The second aspect of this work is about the variation of the Hertzian cone crack semi-included angle in fused silica when it is impacted at normal incidence with 1 mm diameter steel, glass and sapphire spheres in the velocity range 15 to  $340 \text{ m.s}^{-1}$ . It is clear from Figs. 6 and 7 that the semi- included angle of the cone cracks decreases systematically with increasing impact velocity of the projectiles. Moreover, it is shown in Fig. 7 that such

behaviour occurs for all three types of projectile. Previously [16], it was suggested that the Hertzian cone crack angle in Pyrex decreased with increasing impact velocity of the steel spheres because the diameter of the plastically deformed flat on the steel projectiles increased with increasing impact velocity. This meant that after the initiation of a ring crack during the early part of the loading cycle, the radius of contact between the glass and the sphere and the impact load continued to increase with time. The implication of this was that any further growth of the cone crack would occur along sub-surface principal stress trajectories of an increasing steepness to the impacted surface. However, now we have a different view because a close examination of several high-speed photographic sequences has revealed that the included angle of a cone crack formed within about 0.1  $\mu\text{s}$  of the contact does not change at all during the remainder of the loading time. As an example, it will be seen from Fig. 3 (frame 3) that the included angle of  $87^\circ$  of the cone crack formed within 0.1  $\mu\text{s}$  of the impact is exactly the same as the included angle after another  $\mu\text{s}$  (see Fig. 3, frame 4) or even 7  $\mu\text{s}$  later (Fig. 3, frame 10).

We know from Huber's [42] sub-surface stress analysis in the case of the loading of an elastic sphere on an elastic half space that the inclination of the sub-surface principal stress trajectories is dependent upon the Poisson's ratio of the half space and it is the inclination of stress trajectory at  $r \cong a$  (see Fig. 1) that determines the included angle of the Hertzian cone crack. We would, therefore, like to suggest that during an impact the Poisson's ratio of the elastic half space close to the impact site decreases and that the degree of the decrease is dependent upon the impact – generated loading rate. So, the higher the loading rate, the greater will be the decrease in the value of the Poisson's ratio. Support for this suggestion comes from some recent work by Bo et al. [43], who showed that during the dynamic compression of granite specimens at loading rates in the range  $10^0 \text{ MPa}\cdot\text{s}^{-1}$  to  $10^5 \text{ MPa}\cdot\text{s}^{-1}$  the Poisson's ratio of a granite sample containing 3.28 % voids decreased from 0.31 to 0.23 as the loading rate increased from  $5 \times 10^0 \text{ MPa}\cdot\text{s}^{-1}$  to  $10^5 \text{ MPa}\cdot\text{s}^{-1}$ .

We believe that the effect of the loading rate on the Poisson's ratios will also occur for fused silica, Pyrex and soda-lime silica glasses.

Another observation that gives support to our suggestion comes from Fig.7. It will be seen that the data points due to impact with the 1 mm diameter glass spheres lie distinctly above those due to impact with the steel spheres. This means that for the same impact velocity the semi-included angle of the Hertzian cone crack is smaller for a steel-sphere-impact than for a glass-sphere-impact. This observation is consistent with the fact that for the same impact velocity the loading rate for the steel projectiles will be greater than with the glass projectiles, and consequently there will be a greater reduction in the value of the Poisson's ratio for the steel projectiles than will the case for the glass projectiles. It may also be noted from Fig. 7 that for a given projectile impact velocity, the semi included angle of the Hertzian cone produced in fused silica due to a 1 mm diameter sapphire sphere is smaller than that produced with a glass projectile.

The third aspect of this work concerns the total contact time during an impact and the lengths of the cracks generated in different glasses. Table 2 shows that the observed total contact

times when steel projectiles impacted different glasses at velocities in the range 135 – 210 m.s<sup>-1</sup> agree reasonably well with the contact times calculated using Eq. (13). We assume that even at higher impact velocities of 300 to 340 m.s<sup>-1</sup> the loading times for the impacts of 1 mm diameter steel projectiles on to fused silica and soda – lime glass may be similar, though crushing of the glasses is likely to increase the loading times, but because of the ejected debris masking the projectiles, we were not able to measure the loading times. However, from several high-speed photographic sequences we were able to measure and to confirm that in the impacted glasses the cracks of all types travel at or close to their terminal velocities for almost the entire loading times. Therefore, the maximum crack lengths in fused silica and soda-lime glasses will be given by

Maximum crack length in fused silica = Terminal crack velocity in fused silica x loading time,

Maximum crack length in soda-lime glass = Terminal crack velocity in soda –lime glass x loading time.

Now, the loading times in fused silica and soda – lime glass are approximately the same (see Table 2). Therefore the ratio of the maximum crack lengths in the two glasses will be

$$\frac{\text{Maximum crack length in fused silica}}{\text{Maximum crack length in soda-lime glass}} = \frac{\text{Terminal crack velocity in fused silica}}{\text{Terminal crack velocity in soda-lime glass}} \quad (15)$$

Using the maximum measured crack velocities in fused silica given in Table 3 in Eq. (15), we see that the ratio of the maximum crack lengths in the two glasses should be  $\frac{2500}{1500} = 1.66$ .

From Table 3 we obtain the ratio of the maximum crack lengths in fused silica and soda-lime glass as  $\frac{3.44}{2.17} = 1.6$ .

The two ratios are fairly close to each other, suggesting that this method of estimating the particle impact-generated crack lengths is better than using the quasi – static theories (see, for example, Ref. [44]) in which no consideration is given either to the impact loading times or to the crack velocities and in which significant discrepancy is found between the theoretically predicted strength degradation and experimental observations.

The next aspect of our work is the dynamic loading of a tungsten carbide cone of an included angle of 90° on to a block of fused silica at 170 m.s<sup>-1</sup> (see Fig. 10). It is very unusual to see the formation and propagation of a planar median crack in fused silica rather than a Hertzian type conical crack. We believe that in the impact situation at this velocity the fused silica was not able to compact and densify around the tip of the cone and to lead to the formation of a conical crack. It would be interesting to load dynamically a block of fused silica with a similar cone at different velocities and to examine if there is a velocity below which only Hertzian type cone cracks form.

We next consider the loading of a block of soda – lime glass by oblique impact loading (Fig. 8). It is clear from this photographic sequence and others not shown here that a Hertzian cone crack does form on oblique impact, but its orientation is not symmetrical to the normal to the

impacted surface. Instead, the front part (i.e. in the direction of the impact) of the skirt of the cone crack makes a considerably larger angle to the impacted surface than does the rear part of the skirt of the cone crack. This orientation has been found to be similar to the orientation of the Hertzian cone crack in a block of soda – lime glass when the latter is loaded at an oblique angle quasi-statically [34]. As explained in section 4, this type of crack orientation is a result of the geometrical coverage of the front part of the surface ring crack with the contact disc and the uncovering of the rear part of the ring crack due to the sliding of the impacting sphere. Interestingly, the observed cone crack orientation of the cone crack is completely opposite to the orientation proposed in Ref. [33].

Finally, we briefly discuss the absence of bifurcation of fast cracks generated in fused silica, Pyrex and soda-lime silica by small particle impact. We believe that the reason for the cracks travelling even at their terminal velocities, not to bifurcate is that the stress intensity factor driving the cracks is such so as to lead to a stable crack growth. This means that for a given applied load, the cracks would elongate to a fixed distance. On the other hand, when a crack is driven by a tensile stress so that the value of the stress intensity factor increases with increasing crack length, such as in the propagation of cracks within the tension zone of a thermally tempered glass (see Fig. 11), the stress intensity factor increases with increasing crack length until bifurcation occurs and then the bifurcation process repeats again.

## 6. Conclusions

The response of several inorganic glasses to impact with spherical projectiles of diameters 0.8 to 2.0 mm made of different materials has been investigated using high – speed framing photography at rates of up to  $\sim 2 \times 10^6$  frames per second. The glasses were fused silica and ‘Pyrex; (a borosilicate glass), soda-lime glass and  $B_2O_3$ . The first two are ‘anomalous’, whereas the other two are normal types. The projectile materials were steel, glass, sapphire and tungsten carbide. High-speed photography has shown that in the case of the ‘anomalous’ glasses at moderate impact velocities of 200 – 300  $m.s^{-1}$  Hertzian cone cracks initiated at the impacted surface within 0.1  $\mu s$  of the contact being made and then travelled at crack terminal velocities, without any bifurcation, during the remainder of the loading time. In the case of soda-lime glass, fast splinter cracks formed, but  $B_2O_3$  showed compaction and plastic flow.

A new proposal has been made about the decrease of the Hertzian cone angle with increasing projectile impact velocity. According to this proposal, as the loading rate increases with increasing projectile impact velocity, the Poisson’s ratio of the target material decreases accordingly, resulting in a cone crack of a smaller included angle.

In the case of a tungsten carbide conical projectile impacting a block of fused silica, high-speed photography has revealed that a fast planar crack (median type) forms immediately below the apex of the projectile. This observation is quite different from the observation when a Vickers diamond pyramidal indenter is loaded on to fused silica quasi-statically, resulting in the formation of a conical crack. The impact of a wedge-like projectile on a block of soda-lime glass has also been shown to result in a fast planar crack.

It has been argued that particle – impact – generated crack lengths in glasses are a function of the projectile loading time and the terminal velocities of the cracks in the target materials. An example has been provided to support this suggestion.

High-speed photography has also revealed that when a tungsten carbide sphere impacts a block of soda-lime glass at an angle to the surface normal, the Hertzian cone crack formed is not oriented symmetrically to the surface normal, but it is so inclined that the front part of the skirt of the cone crack makes a larger angle with the impacted surface than does the rear part of the cone crack. This has been explained by the sliding of the impacting projectile and covering the surface ring crack in the sliding direction during the formation and growth of the cone crack.

Finally, a high speed photographic sequence has been provided in which the impact of a 2 mm diameter tungsten carbide on thermally tempered glass generates long enough splinter cracks, which penetrate into the tension zone of the block and start a self-sustained crack propagation process, with repeated crack bifurcation. The bifurcation of the cracks in this situation is caused by the residual tensile stress in the specimen for which the stress intensity factor is such so as to lead to an unstable crack growth.

### **Acknowledgements**

I would like to acknowledge sincerely the many stimulating discussions on the phenomena of indentation, fracture and friction which I had over the past 35 years with the late Dr Elizabeth H. Yoffe, who passed away in July 2014. I thank Kelvin Fagan, the Cavendish Laboratory photographer, for his help with the figures.

## References

- [1] Hertz H. 1896 In *Miscellaneous Papers*, translated by D E Jones and G H Schott, Macmillan and Co. Ltd., London. Chapters 5 and 6.
- [2] Auerbach F. 1891 On the absolute measurement of hardness. *Ann. Phys. Chem.* **43**, 61 – 100
- [3] Tolansky S, Howes VR. 1954 Optical studies of ring cracks on glass. *Proc. Phys. Soc. (Lond)* **B 67**, 467 – 472. (doi: 10.1088/0370 - 1301/67/6/303)
- [4] Benbow JJ. 1960 Cone cracks in fused silica. *Proc. Phys. Soc. (Lond)*, **75**, 697 – 699. (doi: 10.1088/0370 -1328/75/5/308)
- [5] Tillett JPA. 1956. Fracture of glass by spherical indenters. *Proc. Phys. Soc. (Lond)*. **B69**, 47 – 54. ((doi: 10.1088/0370 - 1301/69/1/306)
- [6] Roesler FC. 1956. Brittle fracture near equilibrium. *Proc. Phys. Soc. (Lond)*. **B69**, 981 – 992.(doi: 10.1088/0370 – 1301/69/10/303)
- [7] Chaudhri MM, Yoffe EH. 1981 The area of contact between a small sphere and a flat surface. *Philos. Mag.* **A 44**, 667 – 675.
- [8] Wilshaw TR. 1971 The Hertzian fracture test. *J. Phys. D*, **4**, 1567 – 1581. (doi: 10.1088/0022 – 3727/4/10/316)
- [9] Chen SY, Farris TN, Chandrasekar S. 1995 Contact mechanics of Hertzian cone cracking, *Int. J. Solids Structures*, **32**, 329 – 340. (doi: 10.1016/0020 – 7683(94)00127 – 1)
- [10] Jelagin D, Larsson PL. 2008 On indentation and initiation of fracture in glass. *Int. J. Solids Structures*, **45**, 2993 - 3008. (doi: 10.1016/j.ijsolstr.2008.01.008)
- [11] Raman CV. 1919 Percussion figures in isotropic solids. *Nature*, **104**, 113 – 114.
- [12] Benerji K. 1926-1927 On the permanent deformations produced by contact of solids. *Indian J. Phys.* **1**, 59 – 74.
- [13] Andrews JP. 1931 Observations on percussion figures. *Proc. Phys. Soc.* **43**, 18 – 25.
- [14] Chaudhri MM. 1972 Shock initiation of fast decomposition in crystalline solids. *Combustion and Flame*, **19**, 419 – 425. (doi: 10.1016/0010 – 2180(72)90011 – 9)
- [15] Chaudhri MM, Knight CG, Swain MV. 1977 Impact of microparticles on brittle solids. Proc. 12<sup>th</sup> International Congress on High Speed Photography, Toronto 1976. *SPIE*, **97**, 371 – 376.
- [16] Knight CG, Swain MV, Chaudhri MM. 1977 Impact of small steel spheres on glass surfaces. *J. Mater. Sci.* **12**, 1573 – 1586. (DOI: 10.1007/BF00542808)
- [17] Chaudhri MM, Walley SM. 1978 Damage to glass surfaces by the impact of small glass and steel spheres. *Philos. Mag. A* **37**, 153 – 165.

- [18] Chaudhri MM, Brophy PA. 1980 Single particle impact damage of fused silica. *J. Mater. Sci.* **15**, 345 – 352. (doi: 10.1007/BF02396782)
- [19] Chaudhri MM, Kurkjian CR. 1986 Impact of small steel spheres on the surfaces of “normal” and “anomalous” glasses. *J. Am. Ceram. Soc.* **69**, 404 – 410. (DOI: 10.1111/j.1151-2916.1986.tb04769.x)
- [20] Chaudhri MM. 1985 High-speed photographic investigations of the dynamic localised loading of some oxide glasses. In *Strength of inorganic glass* (ed. C. R. Kurkjian), pp. 87 – 113. Plenum, New York. First presented at a NATO Advanced Research Workshop March 21 – 25, 1983 in Algarve, Portugal.
- [21] Chaudhri MM, Wells JK, Stephens A. 1981 Dynamic hardness, deformation and fracture of simple ionic crystals at very high rates of strain. *Philos. Mag. A* **43**, 643 – 664.
- [22] Chaudhri MM, Phillips MA. 1990 Quasi-static indentation cracking of thermally tempered - soda lime glass with spherical and Vickers indenters. *Philos. Mag. A* **62**, 1 – 27.
- [23] Goodier JN, Jahsman WE, Ripperger EA. 1959 An experimental surface wave method for recording force – time curves in elastic impacts. *J. Appl. Mech.* **26**, 3 – 7.
- [24] Hunter SC. 1957 Energy absorbed by elastic waves during impact. *J. Mech. Phys. Solids*, **5**, 162 – 171. (doi: 10.1016/0022-5096(57)90002-9)
- [25] Yoffe EH. 1982 Elastic stress fields caused by indenting brittle materials. *Philos. Mag A* **46**, 617 – 628.
- [26] Boussinesq J. 1885 *Application des potentials a l’E’tude de l’Equilibre et du mouvement des solides E’lastiques*. Gauthier – Villars, Paris.
- [27] Chaudhri MM. 2004 Dislocations and Indentations. In *Dislocations in Solids*, Vol. **12** editors F. R. N. Nabarro and J. P. Hirth, Elsevier, Amsterdam, pp. 447 – 550.
- [28] Tabor D. 1951. *The hardness of metals*, Oxford University Press, Clarendon. P. 132.
- [29] Andrews JP. 1930 LVI. Theory of collision of spheres of soft metals. *Philos. Mag (series 7)* **9**, 593 – 610.
- [30] Chaudhri MM, Hutchings IM, Makin PL. 1984 Plastic compression of spheres. *Philos. Mag. A* **49**, 493 – 503. (doi: 10.1080/014186184082-3655)
- [31] Atkins AG. 1973 High-temperature hardness and creep. In *The science of hardness testing and its research applications*, (editors J. H. Westbrook and H. Conrad) pp. 223 – 240. American Society for Metals, Menlo Park, Ohio. First presented at a symposium of the American Society for Metals, October 18 to 20, 1971.
- [32] Schardin H. 1959 Velocity effects in fracture. In *Fracture* editors Averbach BL, Felbeck DK, Hahn GT, Thomas DA, John Wiley, New York, pp. 297 – 330. First presented at an

international conference on atomic mechanisms of fracture held in Swampscott, Massachusetts, April 12 – 16, 1959.

- [33] Lawn BR, Wiederhorn SM, Roberts DE. 1984 Effect of sliding friction forces on the strength of brittle materials. *J. Mater. Sci.*, **19**, 2561 – 2569. (doi: 10. 1007/BF00550810)
- [34] Chaudhri MM, Liangyi Chen. 1989. The orientation of the Hertzian cone crack in soda-lime glass formed by oblique dynamic and quasi-static loading with a hard sphere. *J. Mater. Sci.*, **24**, 3441 – 3448. (doi: 10 1007/BF02385722)
- [35] Hagan JT. 1979 Cone cracks around Vickers indentations in fused silica glass. *J. Mater. Sci.*, **14**, 462 – 466. (doi: 10. 1007/BF00589840)
- [36] Wiederhorn SM. 1969 Fracture surface energy of glass. *J. Am. Ceram. Soc.* **52**, 99 – 105. (doi: 10. 1111/j. 1151.2916.1969tb13350x)
- [37] Chaudhri MM, Liangyi Chen. 1986 The catastrophic failure of thermally tempered glass caused by small-particle impact. *Nature*, **320**, 48 – 50. (doi: 10.1038/320048a0)
- [38] Davies RM. 1949 The determination of static and dynamic yield stresses using a steel ball. *Proc. Roy. Soc. (Lond) A*, **197**, 416 – 432. (doi: 10: 1098/rspa.1949.0073)
- [39] Gunasekera SP, Holloway DG. 1973 Effect of loading time and environment on indentation hardness of glass. *Phys. Chem. Glasses*, **14**, 45 – 52.
- [40] Peter KW. 1970 Densification and flow phenomena of glass in indentation experiments. *J. Non-Crystalline solids*, **5**, 103 – 113.
- [41] Bridgman PW, Simon I. 1953 Effects of very high pressures on glass. *J. Appl. Phys.* **24**, 405 – 413. (doi: 10. 1063/1.1721294)
- [42] Huber MT. 1904 On the theory of contact of solid elastic substances. *Ann. Physik*, **14**, 153 – 163.
- [43] Bo L, Xiang X, Chong Y. 2013 Dynamic mechanical compression of rock material with different weathering degrees. *Environmental Engineering and Management Journal*, **12**, 1797 – 1801.
- [44] Wiederhorn SM, Lawn BR. 1977 Strength degradation of glass resulting from impact with spheres. *J. Am. Ceram. Soc.* **60**, 451 – 458. (doi: 10. 1111/j.115-2916.1977tb15531.x)

## Figure captions

Fig. 1. Schematic diagram of a Hertzian cone crack, C. C., in an elastic half space produced by the loading of an elastic sphere of radius  $R$  under a normal load,  $P$ . The radius of contact between the sphere and the half space is  $a$ . The radius of the ring crack formed is  $r_c$ , which is shown slightly larger than  $a$ . The diameter of the base of the cone crack is  $S$  and  $\alpha$  is the angle between the skirt of the cone crack and the loaded surface. From Ref. [22].

Fig. 2. (a) Schematic diagram of the side view of the various cracks formed in a brittle solid due to loading it with a hard pyramid of an included angle of  $2\psi$ . The various cracks are: fc – full penny-shaped median crack; hc – half penny-shaped crack, which results on the removal of the pyramid from the surface; lc – a lateral crack also formed on unloading; d – depth of the half penny crack along the load axis. (b) Top view of the two mutually perpendicular median cracks after the removal of the pyramid; the total length of each median crack is  $2c$ ; lateral cracks are not shown. The hatched area under the tip of the pyramid is plastically deformed. From Ref. [22].

Fig. 3. Impact of a 1 mm diameter hardened steel sphere on a block of Pyrex (a borosilicate glass) at  $160 \text{ m.s}^{-1}$ . A cone crack forms in frame 3 and its semi-included angle is  $43.5^\circ$ . In frame 4 a radial crack, R, appears and the cone crack reaches the bottom end of the frame during loading. The rebound of the sphere starts in frame 5 and a lateral crack appears on the left of the impact site and the main cone crack closes up to allow more light transmission through it. Even after the impacting sphere has left the glass, the closing and opening of the crack continues for several microseconds. Interframe time:  $1.0 \mu\text{s}$ . From Ref. [17].

Fig. 4. Impact of a 0.8 mm diameter hardened steel sphere on a block of soda-lime glass at  $300 \text{ m.s}^{-1}$ . Impact occurs between frames 1 and 2, resulting in the formation of fast splinter cracks. Unloading starts between frames 2 and 3, causing lateral cracks (one lateral crack is shown at L in frame 3). Extensive glass debris in frame 3 completely hides the sphere. A chip of detached glass can be seen in frame 12. Interframe time:  $1.0 \mu\text{s}$ . From Ref. [16].

Fig. 5. Impact of a 1 mm diameter hardened steel sphere on a block of  $\text{B}_2\text{O}_3$  glass at  $150 \text{ m.s}^{-1}$ . Impact occurs between frames 1 and 2, resulting in compaction and densification (see at arrow in frame 3) and plastic flow causing pile-up in frame 4. No cracks form during loading. Unloading starts in frame 4 and in the next frame lateral cracks form (one lateral crack is shown at L in frame 6). The sphere leaves the surface of the glass in frame 5 and is followed by a ring of broken off material from the glass surface. Interframe time:  $1.0 \mu\text{s}$ . From Ref. [19].

Fig. 6. Cone cracks in fused silica produced by impact with 1 mm diameter hardened steel spheres at different velocities. (a) Impact velocity:  $25 \text{ m.s}^{-1}$  and semi-included angle of the cone :  $68.5^\circ$ ; (b) Impact velocity  $155 \text{ m.s}^{-1}$  and semi-included angle of the cone :  $46^\circ$ ; (c) Impact velocity :  $310 \text{ m.s}^{-1}$  and semi-included angle of the cone:  $32.5^\circ$ . The width of field is (a) 1.93 mm, (b) 5.27 mm, (c) 5.27 mm. From Ref. [20].

Fig. 7. The variation of the semi-included angle of the Hertzian cone cracks formed in fused silica by the impact of 1 mm diameter projectiles of different materials at different velocities. Solid circles – steel; hollow circles - glass; solid squares - sapphire. From Ref. [20].

Fig. 8. Impact of a 2 mm diameter tungsten carbide sphere on a polished block of soda-lime glass, whose surface normal is inclined to the impact direction at  $60^\circ$ . In frame 1 the arrow shows the impact direction and the velocity of the projectile along the impact direction is  $125 - 150 \text{ m.s}^{-1}$ . The glass block is placed between two circular polarisers. The impact occurs between frames 2 and 3 and in frame 3 the isochromatics formed due to the impact can be clearly seen. A cone crack initiates in frame 3 and becomes well developed in frame 4. Frames 5 – 12 show that the front part of the skirt of the cone crack is tilted at a considerably larger angle to the impact surface than is the rear part of the cone. Interframe time:  $1.0 \mu\text{s}$ .

Fig. 9. Impact of a tungsten carbide cone of a semi-included angle of  $45^\circ$  and base diameter of 1 mm on a block of fused silica at  $170 \text{ m.s}^{-1}$  between frames 1 and 2, resulting in the formation of a sub-surface median crack. No cone cracks form and a fully developed half penny median is shown at M in frame 4. Interframe time:  $0.6 \mu\text{s}$ . From Ref. [18].

Fig. 10. Impact of a tungsten carbide cone of a semi included angle of  $45^\circ$  and of base diameter of 1mm on a polished block of soda-lime glass at a velocity of  $140 \text{ m.s}^{-1}$ . During its 11 mm flight before impacting the glass block, the cone turned on its edge and the wedge-like edge of the cone makes contact with the glass block in frame 3. In frame 4 three planar cracks, 1 – 3, have appeared. Crack 2 is a median type. The cone rotates during the impact, which results in possibly producing a machined chip of glass (see frame 12). Interframe time:  $0.6 \mu\text{s}$ . From Ref.[20].

Fig. 11. Impact of a 2 mm diameter tungsten carbide sphere on a block of thermally tempered soda-lime glass at a velocity of  $150 \text{ m.s}^{-1}$ . The glass block is placed between two circular polarisers, in order to observe the stress-generated isochromatics. The black fringe in frame 1 indicates the position in the glass block at which the residual stress is zero. This black fringe also marks the position at which the residual stress changes from compression to tension. The impact just occurs in frame 3 and in frame 4 splinter cracks initiate and propagate into the tension zone of the block in frame 6. This is followed by self-sustained development and fragmentation of the entire glass block by the process of repeated bifurcation of cracks (frames 7 – 12). Interframe time:  $1.0 \mu\text{s}$ . From Ref. [37]. (colour online).

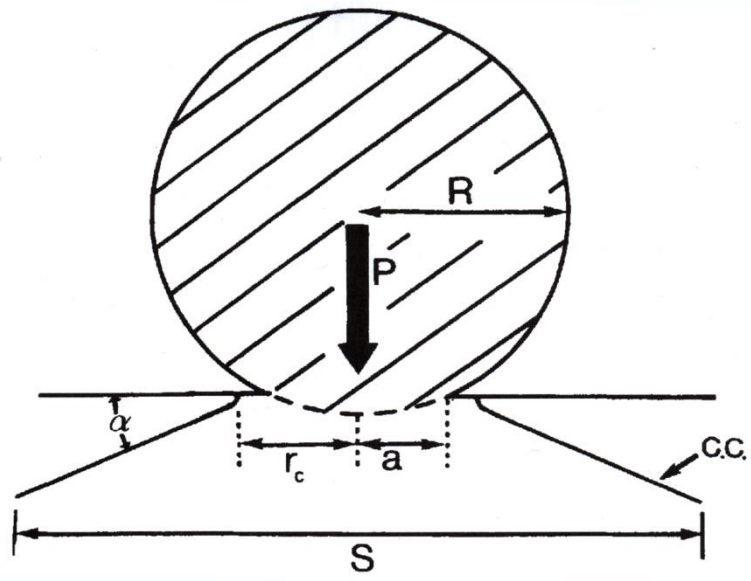


Fig. 1

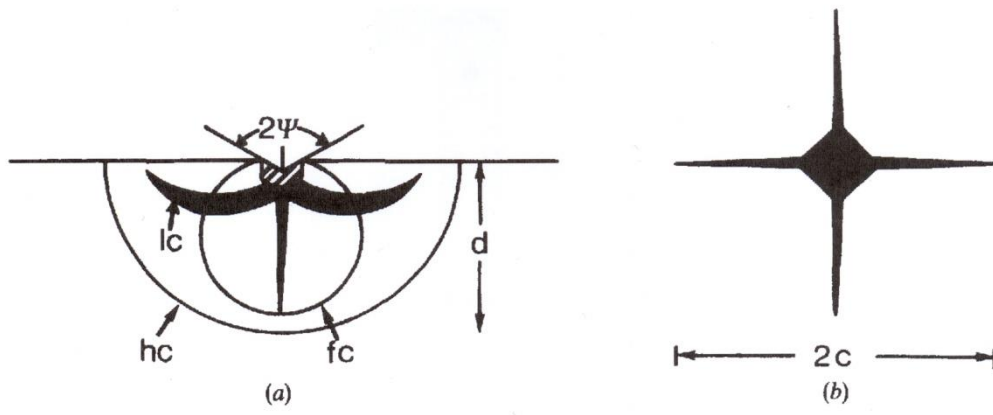


Fig. 2

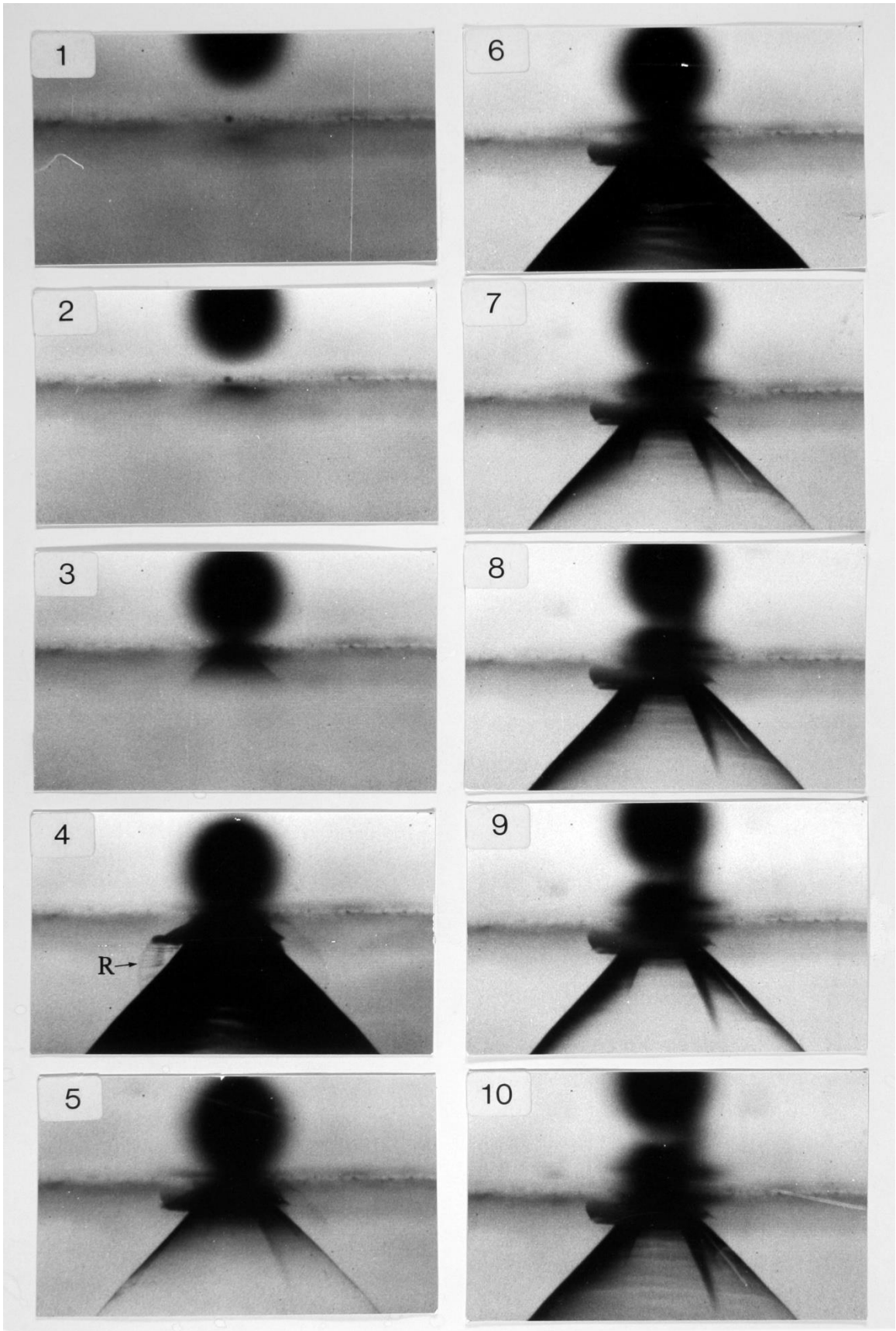


Fig. 3

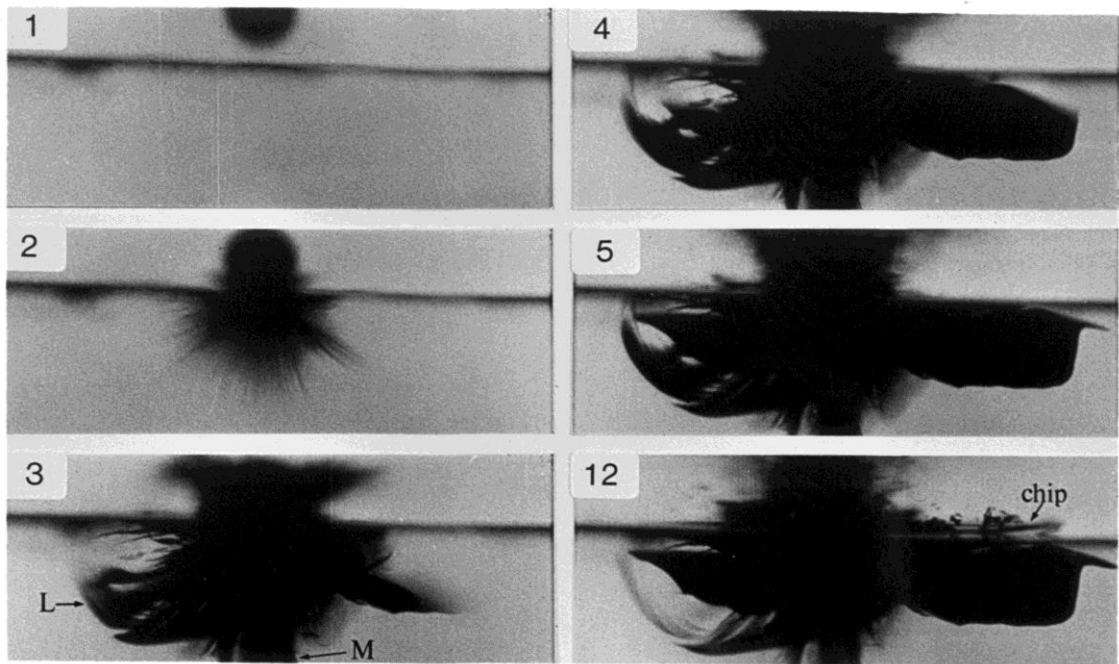


Fig. 4

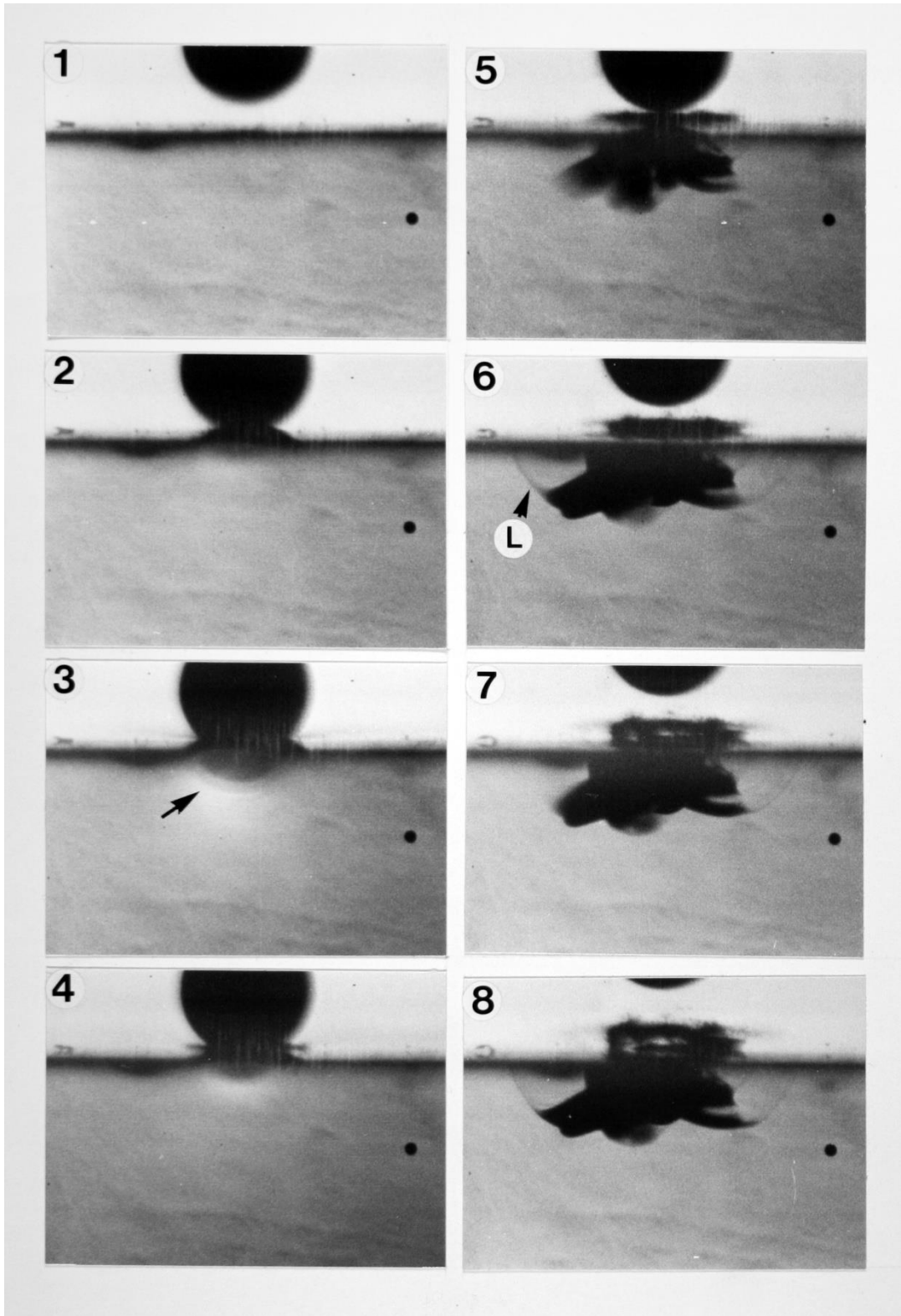


Fig. 5

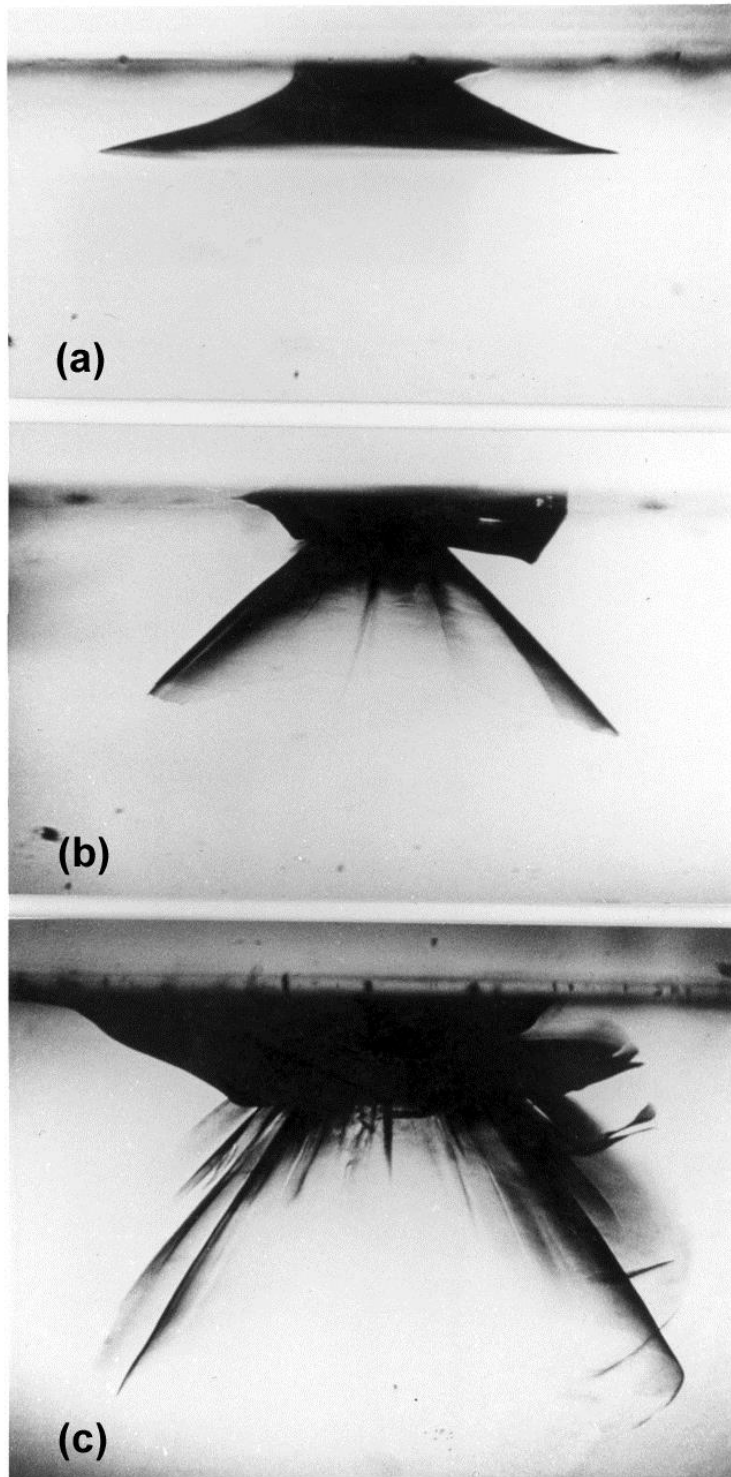


Fig. 6

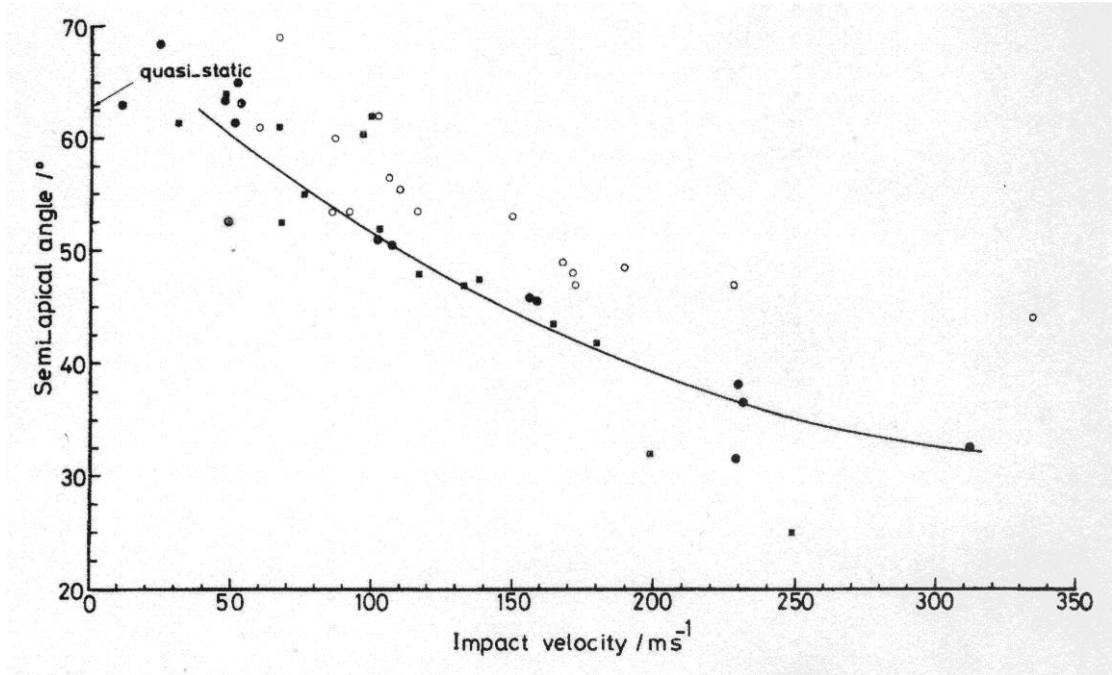


Fig. 7

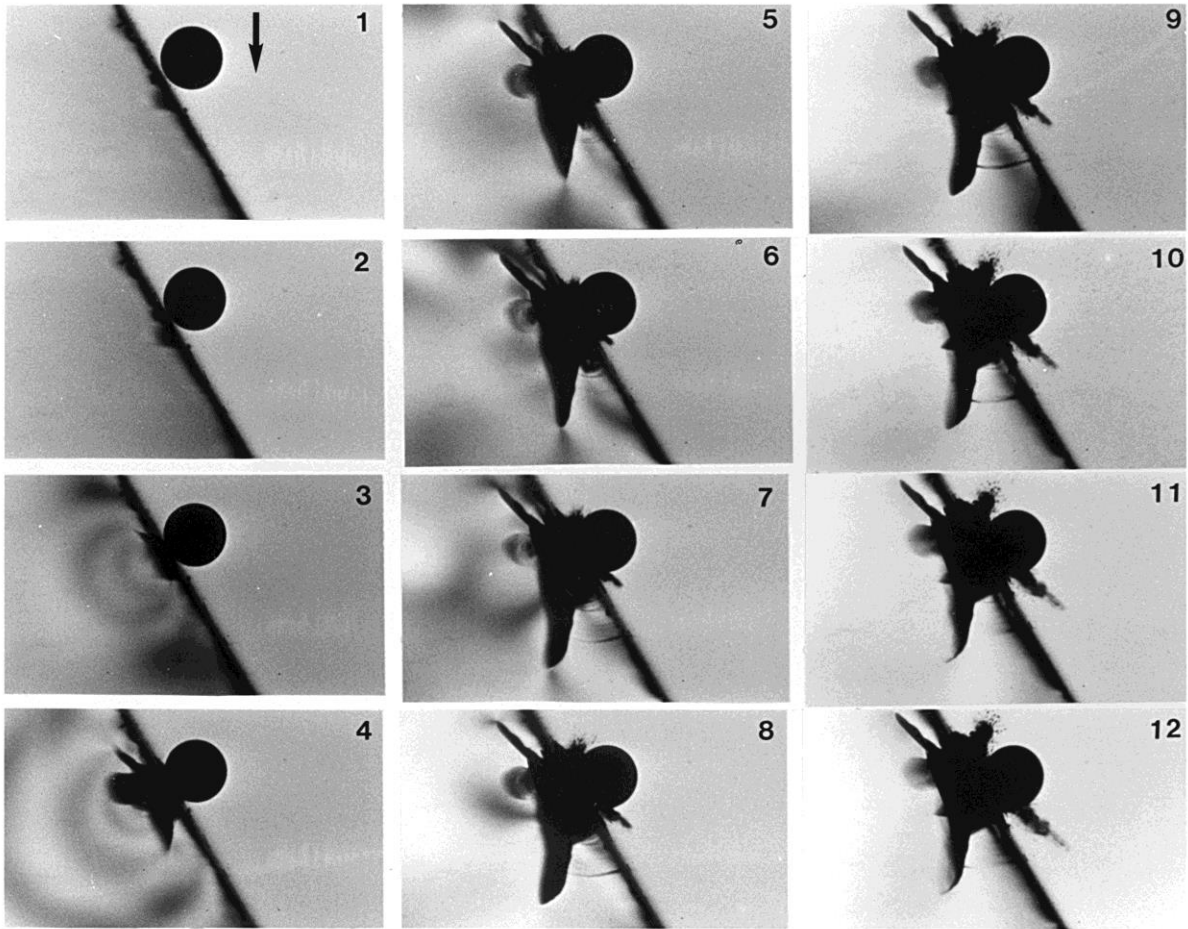


Fig. 8

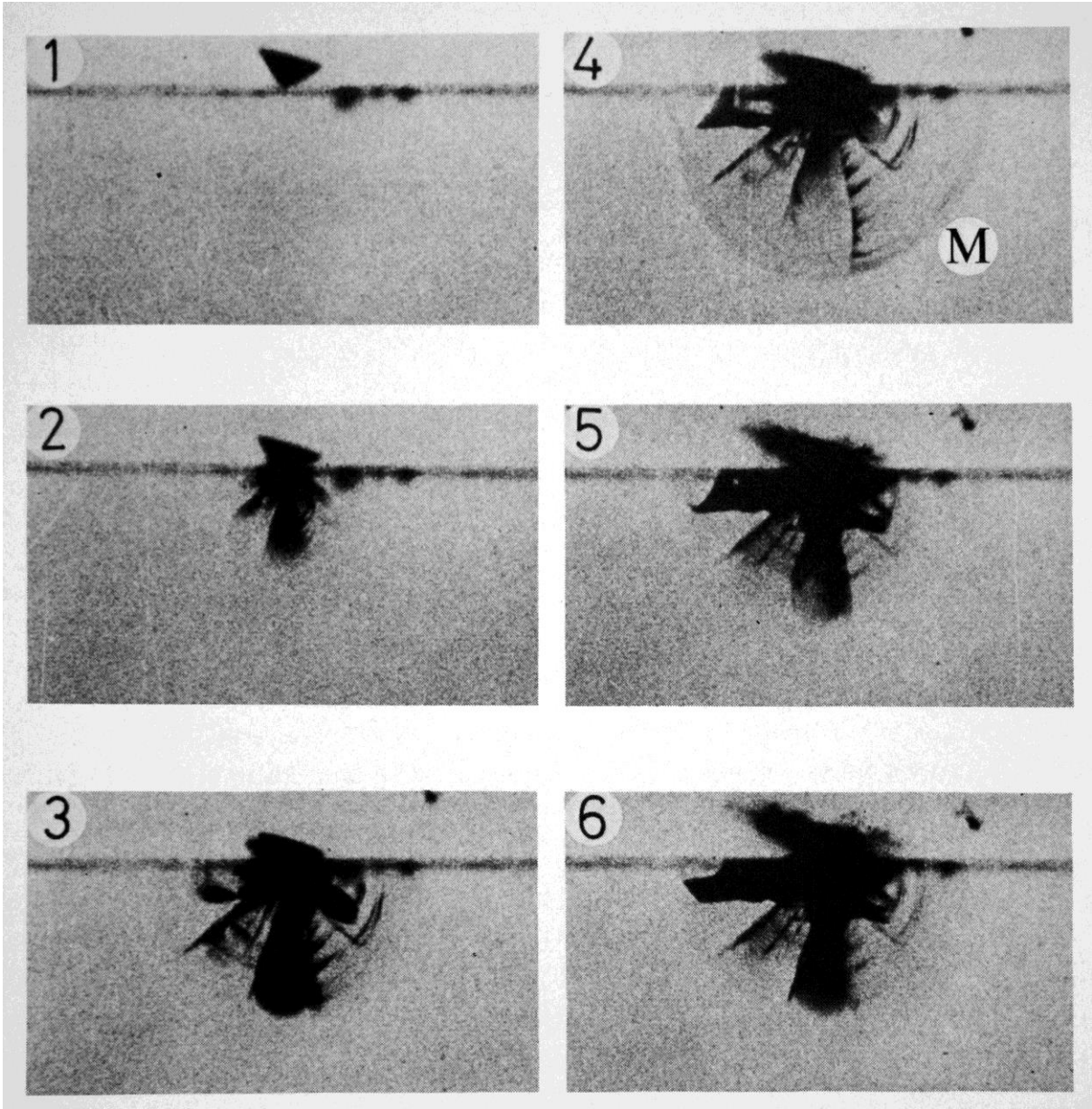


Fig. 9

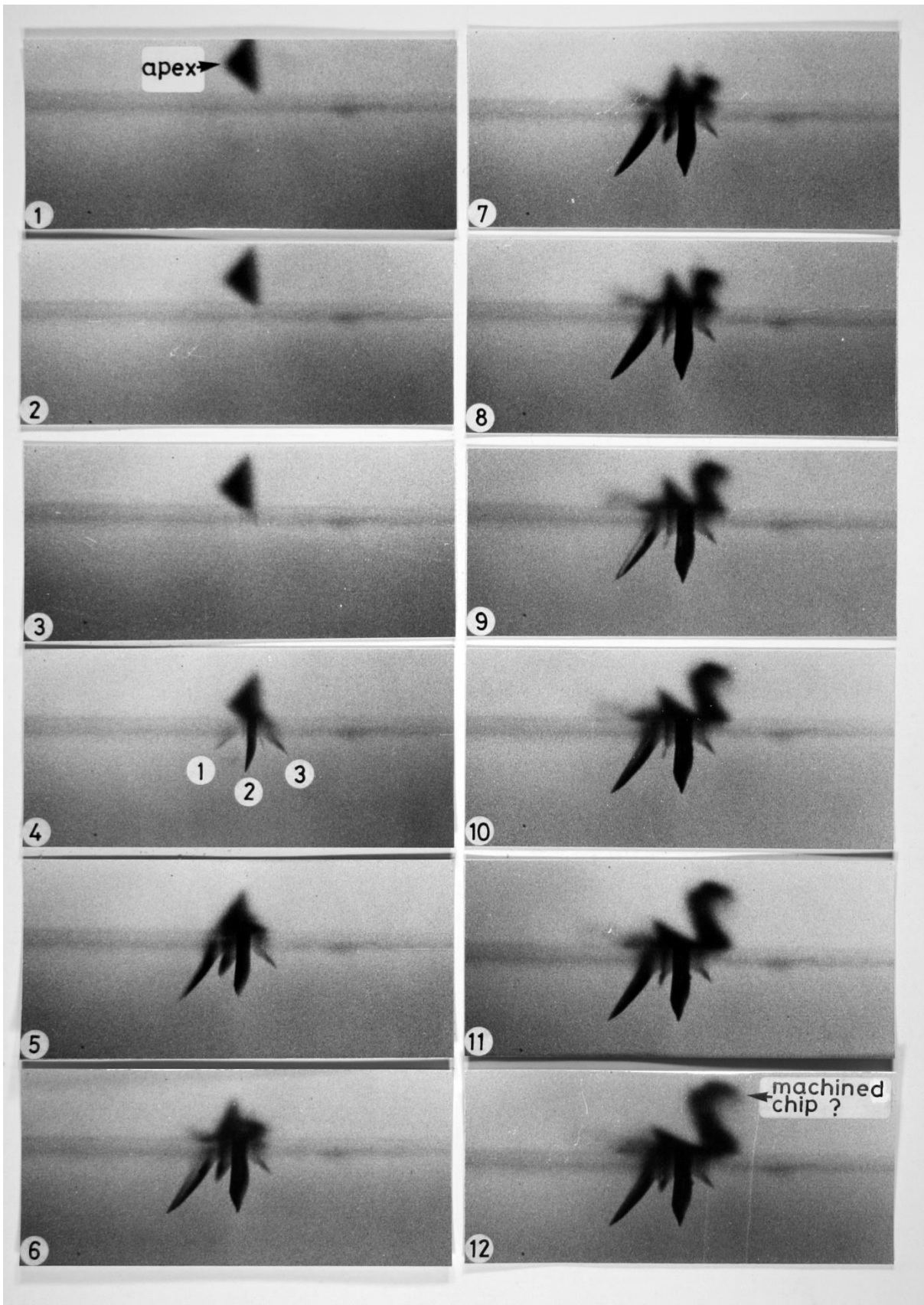


Fig. 10

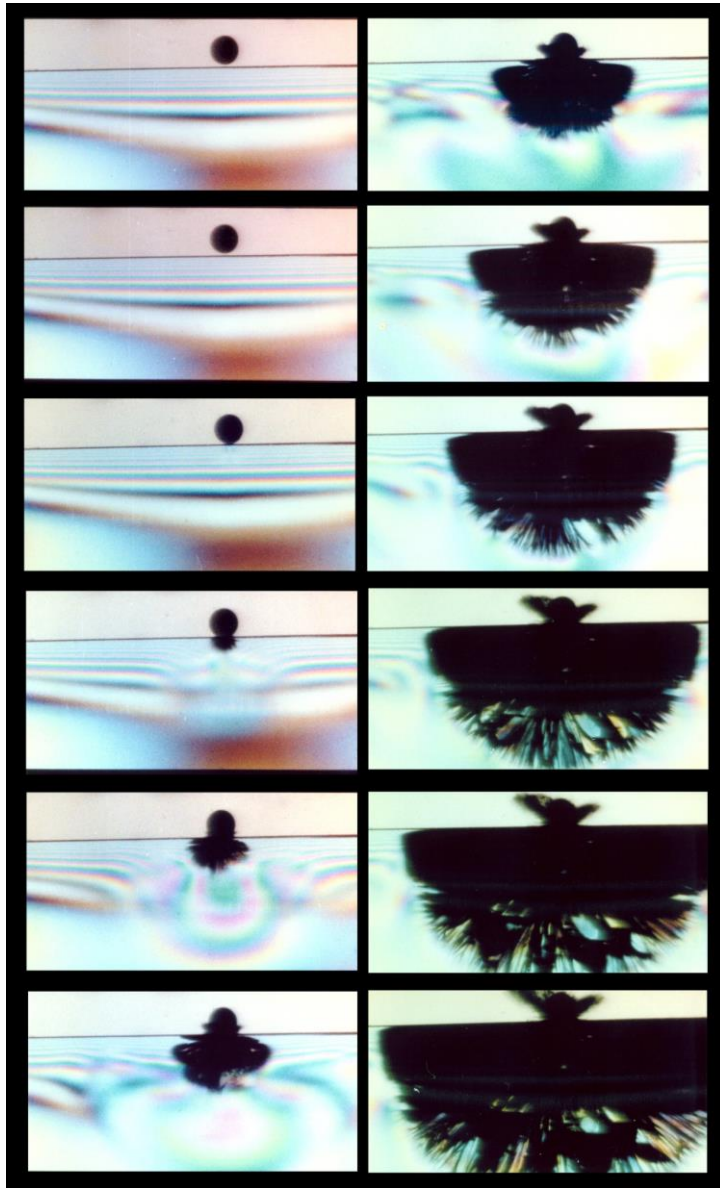


Fig. 11